NASA TECHNICAL MEMORANDUM 102628
AVSCOM TECHNICAL MEMORANDUM 90-B-005

TENSION FATIGUE OF GLASS/EPOXY AND GRAPHITE/EPOXY TAPERED LAMINATES

Gretchen Bostaph Murri, T. Kevin O'Brien, and Satish A. Salpekar

April 1990

National Aeronautics and Space Administration

Langley Research Center
Hampton, Virginia 23665

US ARMY AVIATION SYSTEMS COMMAND
AVIATION R&T ACTIVITY

SUMMARY

Symmetric tapered laminates with internally dropped plies were tested with two different layups and two materials, S2/SP250 glass/epoxy and IM6/1827I graphite/epoxy. Layup A was a $[0_9/(\pm45)_3/(\pm45)_2]_s$ laminate that reduced to a $[0_9/(\pm45)_2]_s$ laminate by dropping the $(\pm45)_3$ plies. Layup B was a $[0_7/\pm45/(\pm45)_3/0/\pm45/0]_s$ laminate that reduced to a $[0_7/\pm45/0/\pm45/0]_s$ laminate in the same manner as layup A. The specimens were loaded in cyclic tension until they delaminated unstably. Each combination of material and layup had a unique failure mode. Calculated values of strain energy release rate, G , from a finite element analysis model of delamination along the taper, and for delamination from a matrix ply crack, were used with mode I fatigue characterization data from DCB tests of the tested materials to calculate expected delamination onset loads. Calculated values were compared to the experimental results. The comparison showed that when the calculated G was chosen according to the observed delamination failures, the agreement between the calculated and measured delamination onset loads was reasonable for each combination of layup and material.

INTRODUCTION

Laminated composite structures with tapered thicknesses are currently being designed as a means of tailoring parts for specific performance requirements. One example of such a structure is a composite rotor hub. Composite hubs are currently being designed and manufactured to be hingeless and bearingless in order to reduce weight, drag, and the number of parts in the hub. In order to achieve the required performance of the flapping-flexure region of the hub, the stiffness of the structure is changed by dropping, or terminating, plies internally in that region. However, these dropped-ply locations create geometric discontinuities that act as sources for delaminations to initiate as the hub undergoes bending and centrifugal tension loads in flight. Although these delaminations may not result in component failure, the low delamination durability of current composite materials may result in high costs for repair or replacement of parts. In order to design more delamination resistant structures, a thorough understanding of the delamination failure is necessary.

Figure 1 shows a schematic of a symmetric laminate with internal plies that terminate, creating thick, tapered, and thin regions in the laminate. In ref. 1, a multi-angle laminate of this type, with an applied tension load, was analyzed using a two-dimensional (2D) finite element (FE) model. The analysis showed that the most likely place for a delamination to originate in such a laminate is at the junction of the tapered and thin sections (point C in fig. 1). As is shown in fig. 2, under a tension load, the continuous belt plies in the tapered region will try to straighten out, resulting in high interlaminar normal stresses at the junction. Reference 1

also showed that the initial delamination growth is almost completely due to interlaminar tension, with the Mode I, or opening mode, component of the strain energy release rate dominant.

In ref. 2, [0°] unidirectional symmetric tapered laminates of three different material types were tested in cyclic tension until unstable delamination failure. The specimens failed by delaminating along the interface between the belt and the underlying plies in the tapered and thin regions (i.e., along ABCD in fig. 1). The failures were always sudden and unstable, with the delamination growing from point C in both directions. The finite element model from ref. 1 was used to calculate strain energy release rates, G, associated with this type of delamination onset, for a range of delamination lengths, for each material tested. The calculated G values increased rapidly as the modeled delamination length increased, until G reached a peak at a delamination length of several ply thicknesses, and then dropped off [2]. The peak calculated G values were then used with mode I fatigue delamination characterization data from double cantilevered beam (DCB) tests to predict delamination onset loads in the test specimens. Predictions based on a delamination growing first into the tapered region were in reasonable agreement with the test results for all three materials, although the predictions were somewhat conservative [2]. This conservatism may have occurred because the actual local taper angle in the test specimens was smaller than the taper angle in the FE model, making the model more susceptible to delamination in the tapered region. It may also be possible that the presence of the large resin pocket inhibited the initial delamination growth in the taper direction so that the initial delamination grew from point C into the thin region. Delamination onset load predictions

assuming initial delamination growth into the thin region were only slightly higher than the calculations for delamination into the tapered region and were in good agreement with the experimental results for all three materials.

In this study, tension fatigue tests were conducted on tapered, multi-angle, composite laminates with internal ply drops. Two layups were tested: a 38-ply $[0_9/(\pm45)_3/(\pm45)_2]_s$ laminate that reduced to a 26-ply $[0_9/(\pm45)_2]_s$ laminate (layup A), and a $[0_7/\pm45/(\pm45)_3/0/\pm45/0]_s$ laminate that reduced to a $[0_7/\pm45/0/\pm45/0]_s$ laminate (layup B). Layup A had only 0° unidirectional plies in the belt region and only ±45° plies in the core. Layup B, however, had a mixture of 0° and ±45° plies in both the belt and core regions. The axial stiffnesses were identical and the bending stiffnesses were similar for these two layups. Two materials were tested with layup A; S2/SP250, a glass/epoxy material, and IM6/1827I, a graphite/epoxy material with a tough interleaf material on one side of each ply. The addition of an interleaf or adhesive layer has been shown to inhibit delamination growth in laminates under static loads [3]. Layup A of the S2/SP250 material was tested in two configurations, with and without a layer of FM73 adhesive at the midplane. Layup B was tested with the IM6/1827I material in two configurations, with and without a layer of interleaf material along the interface ABCD in fig. 1. All specimens were loaded in cyclic tension in a hydraulic test machine until they delaminated. The delaminations occurred suddenly and grew unstably. However, unlike the unidirectional specimens in ref. 2, in this case the delaminations did not always occur at the interface between the belt and core plies. The presence of the ±45 degree plies in these

laminates resulted in matrix ply cracking which then led to delamination of the adjacent interfaces. Each combination of layup, material and interleaf placement had a slightly different failure mode.

In this study, for those laminates that delaminated along interface ABCD, delamination onset was predicted, as in ref. 2, using the calculated strain energy release rate values from the FE analysis and the mode I fatigue characterization data for the tested materials. For laminates with delaminations from matrix cracks, the observed failure was modeled and G was calculated from a solution for the strain energy release rate associated with local delaminations from matrix ply cracks. Those calculated G values were used with the fatigue characterization data to calculate expected delamination failure loads.

NOTATION

a	delamination length along taper
b	delamination length in thin region
E_{LAM}	modulus of a laminate with no damage
E_{LD}	modulus of a locally delaminated laminate cross-section
h	thickness of one ply
G	total strain energy release rate
G_I	mode I strain energy release rate
G_{II}	mode II strain energy release rate
G_{Imax}	mode I cyclic strain energy release rate
G_{12}	shear modulus

m	number of delaminations associated with a matrix ply crack
n	number of plies in undamaged laminate
n_{LD}	number of unbroken plies in locally delaminated laminate cross-section
N	number of loading cycles to delamination onset
N_x	load per unit width on symmetric half-thickness laminate
P	load applied to symmetric laminate
P_{max}	maximum cyclic load on tapered laminates
R	ratio of minimum to maximum applied load
t	laminate thickness
t_{LD}	thickness of a locally delaminated laminate cross-section
w	specimen width
β	taper angle
ν_{12}	Poisson's ratio
σ_o	applied tensile stress on thick end of laminate
σ_n	interlaminar normal stress
τ_{nt}	interlaminar shear stress
V_f	laminate fiber volume fraction

EXPERIMENTS

Materials

Two different materials were used in the study: IM6/1827I graphite/epoxy and S2/SP250 glass/epoxy. The S2/SP250 is a 250°F cured glass/epoxy prepreg manufactured by 3M. The IM6/1827I is a 350°F cured graphite/epoxy/interleaf prepreg manufactured by American Cyanamid. The IM6/1827I material has a tough thermoset adhesive, or interleaf layer, on one side of the prepreg material. Tapered panels of each material were laid up at NASA Langley using a tool supplied by Bell Helicopter Textron which yielded a panel that had a thin region near the two edges and a thicker region in the center. The thickness change is accomplished by dropping internal plies. Figure 3 shows a drawing of a laminate cut from a cross section of such a panel. One inch wide strips were cut from the panel, and then were cut in half cross-wise to form two test specimens, each ten inches long. Figure 4 shows a schematic of the upper half of the laminate. The thick, tapered and thin regions each have a nominal length of 60h, where h is the ply thickness. The interior plies that run the length of the laminate were designated the core plies and the exterior plies that also run the length of the laminate were called the belt plies. The taper is created by terminating, or dropping, pairs of ± 45 degree plies at three locations. These pairs are dropped at intervals of 20h, yielding a taper angle, β , of 5.71°. At the end of each dropped ply pair, a resin pocket of triangular cross section was assumed to form. In ref. 2 it was shown that fig. 4 is an idealized approximation of the tapered laminate. In the actual test

specimens the two plies of a dropped pair may not be exactly aligned with each other, or the dropped plies may not be aligned with the corresponding dropped pair on the other side of the specimen midplane. It was also noticed that during the curing process some of the belt plies and core plies expanded to allow easier resin flow, or assumed a curvature to allow a smoother transition from the thick to thin regions. This resulted in smaller local taper angles at the tips of the resin pockets than in the tapered laminate model. The laminates tested in this study showed similar manufacturing flaws. Figure 5 shows a photograph of the tapered region of an IM6/1827I, layup A specimen. The dropped ply locations are not symmetric about the midplane, and the two dropped plies are not always aligned.

Two different layups were used in this study. Layup A was a $[0_9/(\pm45)_3/(\pm45)_2]_s$ laminate that reduced to a $[0_9/(\pm45)_2]_s$ in the thin section by dropping the group of three (±45) plies. Layup B was a $[0_7/(\pm45)/(\pm45)_3/0/(\pm45)/0]_s$ laminate that reduced to a $[0_7/(\pm45)/0/(\pm45)/0]_s$ laminate in the same manner as layup A. Layup A was tested with the IM6/1827I and S2/SP250 materials. The layup A S2/SP250 specimens were tested in two configurations, with and without a layer of FM73 adhesive at the midplane, to suppress midplane delaminations. Layup B was tested with only the IM6/1827I material, but in two configurations. Because the IM6/1827I prepreg material has interleaf on only one side, the location of the interleaf material in the laminate can be varied. Therefore, one panel was manufactured so that the interleaf was toward the specimen midplane in every ply, as shown in fig. 6(a), where the arrows indicate the location of the interleaf in the ply. As fig. 6(a) shows, this

stacking sequence provides a layer of interleaf at every interface, including interface ABCD. The second panel was made with the interleaf oriented as shown in fig. 6(b), so that there is no interleaf along ABCD and there is a double layer between the 0 and 45 degree belt plies and between each pair of dropped plies. There is no interleaf along GF'D, the interface between the core and the dropped plies.

Static Tests

Two specimens of each layup and material combination were tested statically to determine the elastic moduli of the thin and thick regions. The specimens were instrumented with extensometers and loaded in a servo-hydraulic load frame. Figure 7(a) shows a specimen in the load frame, with the two extensometers mounted over the thin and thick regions. Specimens were loaded in stroke control at 0.01 inches/minute and the load and displacement were recorded on an X-Y-Y' recorder.

Fatigue Tests

Tapered specimens were instrumented with an extensometer mounted over the tapered region to detect delamination onset, and were then loaded in a servo-hydraulic load frame. Figure 7(b) shows the specimen in the load frame, with the extensometer attached. Specimens were loaded statically to the mean load and were then cycled sinusoidally at a constant load amplitude, at a frequency of 5 Hz and an R ratio of 0.1. This R ratio was chosen to be consistent with the work done in refs. 2 and 9 and represents a severe loading cycle. Specimens were cycled until the onset of delamination, which was always unstable. Delamination was detected either

visually, audibly, or by monitoring the voltage output of the extensometer to detect a change in displacement in the tapered region. If a prescribed displacement change was exceeded, the function generator stopped the loading, and the number of loading cycles was recorded. Using this technique, tests could be run unattended and the machine would detect the onset of delamination. For each configuration, tests were run at several load levels to determine the number of cycles to delamination onset as a function of the applied maximum cyclic load. Table 1 lists the different combinations of material and layup tested, and the number of test specimens of each.

ANALYSIS

Finite Element Model

In ref. 1, a 2D finite element model of a half-thickness symmetric tapered laminate of the type shown in fig. 4, with layup B, was developed. Because the laminate is symmetric about the midplane, it is necessary to model only half the laminate. The model was used to determine the strain energy release rate associated with delamination growth originating at point C and growing toward the thin or tapered regions along interface ABCD. For a symmetric laminate, this corresponds to a delamination at both interfaces ABCD. The model used 8-noded, isoparametric parabolic elements for which the smallest element size was one-quarter ply thickness, or h/4. The mesh was refined in the vicinity of the ply drops and at point C. Collapsed 8-noded elements were used at the tips of the resin pockets. At the end of the thin region the nodes were constrained in both the x- and z-directions, and a uniform load per unit width of N_x=1000 lb./in. was applied to the

thick end. Because the continuous belt plies are at an angle β to the global coordinate system in the tapered region, the moduli of the belt plies must be transformed through the taper angle. This transformation is explained in ref. 2.

To simulate delaminations along interface ABCD, duplicate nodes were created in the model along this interface and were constrained to act together. Different delamination lengths were then modeled by releasing the appropriate nodal constraints. Normalized total strain energy release rates, Gh/N_x^2, were calculated for models with different delamination lengths using the virtual crack closure technique (VCCT) [4]. This technique also calculates the individual mode I (opening) and mode II (shear) components of the strain energy release rate , G_I and G_{II}. The normalized Gh/N_x^2 term is used rather than G, to make comparisons with laminates with other thicknesses and loading easier. Further details of the finite element model analysis are given in ref. 1.

Delaminations from Matrix Ply Cracks

Strain energy release rates were also calculated for delamination growth from matrix ply cracks in the tapered laminates. When matrix ply cracks exist in the off-axis plies of a laminate, delaminations may form in the adjacent interfaces. In ref. 5, a solution for G for delaminations from matrix ply cracks was developed. This analysis was used to predict delamination onset from matrix ply cracks in fatigue for flat laminates [6]. The analysis assumes that the laminate contains a matrix ply crack through a fixed number of off-axis plies, and delaminations then form at the crack tip

and grow in the ply interfaces, as shown in fig. 8(a). Reference 5 gives the expression for G as,

$$G = \frac{P^2}{2mw^2}\left(\frac{1}{t_{LD}E_{LD}} - \frac{1}{tE_{LAM}}\right) \tag{1}$$

where m is the number of delamination planes growing from the matrix ply crack observed on any section A-A, as shown in fig. 8(b). In this study, m=1 for all the observed failures. The thickness and modulus of the undamaged laminate are t and E_{LAM}, and t_{LD} and E_{LD} refer to the thickness and modulus, respectively, of the locally delaminated region, i.e., the thickness and modulus of the portion of the laminate without broken plies. (See fig. 8(a).) As eq. (1) shows, the magnitude of G for a delamination originating at a matrix ply crack does not depend on the size of that delamination, however, t_{LD} and E_{LD} depend on the location of the delamination and the layup of the laminate. The derivation of eq. (1) is given in detail in ref. 5. In ref. 7, eq. (1) was shown to be valid where the matrix cracks intersect the free edge, rather than in the interior.

In order to be able to compare the calculated G values for delamination from a matrix ply crack with G from the 2D FE analysis for delamination along the taper, eq. (1) was rewritten to give Gh/N_x^2. Since N_x is the maximum cyclic load per unit width on the tapered laminate half-thickness, the maximum cyclic load on the tapered laminate is

$$P = 2\,w\,N_x \tag{2}$$

where w is the laminate width. Substituting eq. (2) in eq. (1) and rearranging gives

$$\frac{Gh}{N_x^2} = \frac{2h}{m}\left(\frac{1}{t_{LD}E_{LD}} - \frac{1}{t\,E_{LAM}}\right) \tag{3}$$

as the normalized strain energy release rate for delamination from a matrix ply crack. Letting n and n_{LD} represent the number of plies in the laminated and locally delaminated cross-section, respectively, the thicknesses t and t_{LD} can be expressed in terms of the ply thickness h as $t=nh$ and $t_{LD}=n_{LD}h$. Equation (3) can then be written as

$$\frac{Gh}{N_x^2} = \frac{2}{m}\left(\frac{1}{n_{LD}E_{LD}} - \frac{1}{n\,E_{LAM}}\right) \tag{4}$$

RESULTS AND DISCUSSION

Experiments

Table 2 lists material properties for the test materials as determined in ref. 2. The properties listed for the IM6/1827I represent smeared properties for the fiber-reinforced epoxy plus the interleaf material. Table 3 lists the average measured longitudinal moduli of the thin and thick regions of the tapered laminates for each configuration tested. Table 3 also lists the average measured ply thicknesses of the thin and thick regions and calculated moduli from laminated plate theory (LPT) for the thin and thick sections, using the material properties in Table 2. The LPT moduli agree closely with the measured values for the IM6/1827I laminates

and the S2/SP250 laminates with adhesive at the midplane. The S2/SP250 laminates without adhesive had higher fiber volume fractions than the material in ref. 2 (Table 2), and consequently had slightly higher moduli than the LPT calculations.

For all the tested specimens, the delamination was sudden and unstable. However, each unique combination of layup and material exhibited a slightly different failure mode. For layup A of the S2/SP250 material the onset lives were similar for both the specimens with and without the FM73 adhesive at the midplane; however, both types of specimen showed a variety of failure modes. In most of the laminates, the delamination occurred on both sides of the midplane, on the taper along ABCD, as shown in fig. 9(a). In some cases, there was, in addition to this delamination, a ply crack in the 45 degree core ply and a delamination between the 45 and -45 degree plies in the thin region, as shown in fig. 9(b). The ply crack was always located in the thin region or under point C. In other cases there was a ply crack in the 45 degree ply, between points C and F', or at F', that extended into the resin pocket, as shown in fig. 9(c). One specimen of each configuration showed this type of ply crack, but the delamination extended only along BF, and not along FC. Also, in one specimen of each configuration, this crack was present with no delamination.

For the layup A specimens of IM6/1827I material, delaminations occurred only on one side of the laminate mid-plane and the delamination was always between the core plies. The delaminations originated from a matrix ply crack that could occur at several possible locations. Seven of the laminates showed matrix ply cracks in the thin region, in any of the ±45 plies except the double -45 plies at the midplane; fig. 10(a) illustrates a

typical case. In four other specimens there was a matrix ply crack in a -45 degree core ply within the tapered region, as in fig. 10(b). In two laminates there was a matrix crack in the innermost dropped -45 degree ply, as shown in fig. 10(c).

The delamination onset load vs. number of loading cycles for the IM6/1827I layup B laminates with and without interleaf at ABCD is shown in fig. 11. As the figure shows, the specimens with the interleaf at ABCD exhibited much longer delamination onset lives than did the specimens without the interleaf. The damage mode was also different for the two configurations. For the specimens with the interleaf, delamination occurred only on one side of the midplane in every case. For every specimen there was a matrix crack present in the -45 belt ply and a delamination at the 45/-45 interface in the belt. The crack was located in the thin region, slightly ahead of point C for four laminates (fig. 12(a)), and was in the taper region above the first resin pocket for four laminates, (fig. 12(b)).

For the Layup B specimens without the interleaf material along ABCD, half the specimens delaminated on both sides of the midplane and half delaminated only on one side. Six of the laminates showed a matrix ply crack in the innermost -45 degree dropped ply, with a delamination between the dropped -45 ply and the 0 degree core ply, which extended into the thin region, as shown in fig. 13(a). Two of these six laminates had this damage only on one side of the midplane. In the other four, there was also damage on the other side of the midplane. In these laminates there was a matrix ply crack in the -45 belt ply in the thin or tapered region and a delamination between the 45 and -45 degree belt plies in the tapered and thin regions, as shown in fig. 13(b). The remaining two laminates of this

configuration had a matrix ply crack in the -45 belt ply in the thin region with a delamination at an adjacent interface, as was shown in fig. 12(a).

Table 1 lists the different test configurations and the number of specimens of each with the failure modes shown in figs. 9, 10, 12, and 13. There was no correlation between the delamination onset life and the observed failure mode for any configuration.

Finite Element Analysis

The 2D finite element model was used to calculate interlaminar stresses along interface ABCD and strain energy release rates associated with delamination growth from point C in fig. 4 along CB and CD. The material properties in Table 2 were used in all calculations in the current study. The neat resin properties in Table 2, from ref. 8 were used to model both materials. The adhesive layer was not modeled in the S2/SP250 layup A laminates. Figures 14-16 show σ_n/σ_o, the interlaminar normal stresses along ABCD normalized by the applied stress, for the S2/SP250 layup A, and the IM6/1827I material, layups A and B, respectively. Since the FE model uses smeared properties for the reinforced epoxy ply with the interleaf for the IM6/1827I material, fig. 16 corresponds to a laminate with interleaf at every interface. The results in figs. 14-16 are consistent with the results of refs. 1 and 2, in that the stresses reach a maximum at point C and are tensile on both sides of C, indicating that a delamination along this interface is most likely to initiate at point C. The steep peaks at the dropped ply locations suggest that the interlaminar stresses may be singular there. Figures 17-19 show the normalized interlaminar shear stresses, τ_{nt}/σ_o, along the same interface, for the S2/SP250 layup A laminates. The

shear stresses show high peaks at the dropped ply locations for all three configurations, as did the results of refs. 1 and 2.

For each specimen configuration, the finite element analysis was used to calculate the strain energy release rate for a delamination growing from point C, either along interface ABC in the taper, or along interface CD in the thin region. Delaminations along ABC were designated of length a, and delaminations along CD were designated of length b. At each delamination length, a normalized G was calculated. Figures 20-22 show the calculated values of Gh/N_x^2 for the S2/SP250 layup A, the IM6/1827I layup A, and the IM6/1827I layup B, respectively. As figs. 20-22 show, for all three configurations, and for delaminations in both directions, the calculated values rise steeply and reach a peak at a delamination length of a few ply thicknesses, and then drop as the delamination continues. In each case, as well, the peak value is higher for delamination growth in the tapered region. Assuming that the toughness is the same in both directions, i. e., neglecting the increasing thickness of the resin pocket, this indicates that the delamination is most likely to grow first in the tapered direction. Figure 23 shows the ratio of G_I to total G for the three configurations. As the figure shows, for all three configurations the initial delamination growth is primarily mode I for growth either into the thin or tapered regions.

The results of the finite element calculations for the configurations modeled in this study agree qualitatively with the results of refs. 1 and 2 for a delamination growing from point C, along ABCD in a tapered laminate with no damage. The consistency of results for all three studies indicates

that the tendency to delaminate along ABCD is a result of the taper geometry, and does not depend on the layup or material modeled. Although delamination along ABCD was observed in this study only for the S2/SP250 laminates, results were included for all the configurations for completeness.

Delamination at Belt Interface

In ref. 9, the mode I delamination fatigue behavior of S2/SP250 and IM6/1827I material was characterized using the double cantilevered beam (DCB) test. Each DCB specimen was tested only until delamination growth was detected. By testing a series of specimens at a variety of load levels, a plot relating G_{Imax} at delamination onset to the corresponding number of loading cycles, N, was generated. For example, fig. 24 shows results for the IM6/1827I material, both with and without interleaf at the delaminating interface. The results for both materials are given in ref. 9 and are listed in Tables 4-7 for S2/SP250, IM6/1827I with interleaf at the delaminating interface, and IM6/1827I without interleaf at the delaminating interface. In ref. 2, these G-N data and the peak Gh/N_x^2 values calculated from the finite element model were used to predict delamination onset load in 0° tapered laminates of the same three materials. Because the finite element analysis showed that the initial delamination growth from point C was predominantly mode I for delamination growth in either direction, it was deemed sufficient to use mode I fatigue data in the calculations. Predictions calculated assuming delaminations grew first into the tapered region were reasonably accurate for each case, although slightly

conservative [2]. However, even though the higher peak value of Gh/N_x^2 corresponded to delamination growth into the tapered region for all three materials modeled, the thick resin pocket may actually have inhibited the initial delamination growth in this direction. Predictions calculated assuming the delamination grew into the thin region first, showed good correlation with the test results for each material. However, in the current test results, only the S2/SP250 laminates showed a tendency to delaminate along interface ABCD as modeled by the FE analysis. Therefore, predictions were calculated and compared to the experimental results for the S2/SP250 laminates only.

To predict delamination onset in the tapered laminates, it was postulated that delamination onset from point C would occur in the laminates when the total G value calculated from the FE analysis equaled the cyclic G_{Imax} at which delamination initiated in the DCB tests. Delamination onset loads were predicted using the following equation,

$$P_{max}(N) = 2w \left[\frac{G_{Imax}(N)\, h}{\left(\frac{Gh}{N_x^2} \right)_{FE}} \right]^{1/2} \qquad (5)$$

where w is the laminate width, h is the average measured ply thickness, and $P_{max}(N)$ is the maximum cyclic load on the tapered laminate at which delamination is expected to occur after N loading cycles. For each value of N in Table 4, the corresponding G_{Imax} was used in eq. (5) to solve for the predicted maximum cyclic load P_{max}. Table 4 lists the calculated values for delamination initiation in the thin and in the tapered regions, where

the $(Gh/N_x^2)_{FE}$ values are the peak values from fig. 20 for delamination onset in the specified direction.

Figure 25 compares the measured delamination onset loads with the predictions for delamination onset in the tapered and thin regions for the S2/SP250 laminates. As the figure shows, the presence or lack of adhesive at the midplane in the tested laminates did not affect delamination failure load. This was expected since none of the failures occurred at the midplane. The figure also shows very good agreement between the test results and the predictions for this case. The predictions for delamination onset in the tapered region are slightly lower than for onset in the thin region.

Delamination from Matrix Ply Cracks

In this study, none of the IM6/1827I laminates failed along ABCD as modeled in the FE analysis. Rather, the delaminations were always associated with matrix ply cracks and were always at locations other than interface ABCD. Therefore, for those laminates, delamination onset loads were determined using G calculated from eq. (1) for delaminations from matrix ply cracks. These calculated failure loads were compared with the experimental results. The variables t_{LD}, E_{LD}, and m were determined by modeling the failure modes that were observed most frequently for each configuration (figs. 10(a, b, c), 12(a, b), and 13(a)).

Delamination onset loads were calculated using the solution for total G for a delamination from a matrix ply crack. It has been shown [10-12], that for long term fatigue behavior of composites with mixed mode

delaminations, delamination growth is characterized by a total G criterion, rather than a more general criterion requiring computation of the individual mode components. Furthermore, the G_{Imax} data in Tables 4-7 also represents the total G_{max}. The criterion for fatigue delamination onset from a matrix crack becomes $G_{max} = G_{Imax}(N)$. Substituting $G_{Imax}(N)$ for G in eq. (1) and solving for $P=P_{max}(N)$ gives

$$P_{max}(N) = \left[\frac{2\, m\, w^2\, G_{Imax}(N)}{\left(\frac{1}{t_{LD} E_{LD}} - \frac{1}{t\, E_{LAM}} \right)} \right]^{1/2} \qquad (6)$$

where the thickness and modulus of the locally delaminated region, t_{LD} and E_{LD}, and the coefficient m, depend on the number and location of delaminations modeled. For example, for the IM6/1827I specimens with layup A, with a crack in the outer -45 degree core ply in the thin region and a single delamination at one of the adjacent interfaces (fig. 10a), t is the total laminate thickness (t=26h), t_{LD} is the thickness of the unbroken plies (t_{LD}=25h), and E_{LD} is found using the rule of mixtures solution for a $[0_9/45]$ laminate in parallel with a $[45/(-45)_2/45/-45/45/0_9]$ laminate. The normalized strain energy release rate from eq. (4) was calculated to be 60.4×10^{-12} in^2/lb for delamination from a matrix ply crack in the outer 45 degree core ply in the thin region (fig. 10a). For a ply crack located in the tapered region (fig. 10b), the properties of the belt plies must be transformed through the taper angle. For the same 45 degree cracked ply in

this region, eq. (4) gives $Gh/N_x^2 = 87.4x10^{-12}$ in^2/lb. For a crack in the innermost dropped -45 degree ply (fig. 10c), $Gh/N_x^2 = 94.2x10^{-12}$ in^2/lb, where the thicknesses are taken at the location of the crack, ignoring the resin thickness; i.e., t=30h and t_{LD}=29h. The calculated failure loads from eq. (6) for the IM6/1827I laminates with layup A are tabulated in Table 5. Figure 26 compares the calculated results for a core ply matrix crack in the thin region with the experimental results. The calculated values correlate very well with the experimental values. The results are compared with the solution for a core ply matrix crack in the tapered region in fig. 27. In this case the calculated values are slightly conservative compared to the experimental values. The tabulated values in Table 5 for delamination onset load from a matrix crack in the dropped ply are slightly less than for a core ply matrix crack in the thin region.

For the IM6/1827I layup B laminates with interleaf at ABCD, fig. 12(a) shows that the specimens always contained cracks in the -45 degree belt ply and a delamination between the 45 and -45 degree plies in the belt. For a tapered laminate with a matrix crack between points F and C in the -45 degree belt ply, $Gh/N_x^2 = 75.2x10^{-12}$ in^2/lb, where again the belt ply properties must be transformed through the taper angle, β. For a matrix crack in the -45 degree belt ply in the thin region, $Gh/N_x^2 = 52.6x10^{-12}$ in^2/lb. Figure 28 shows the experimental results for layup B with interleaf, and the calculated failure loads for delamination onset from a matrix ply crack in the belt ply in the thin region, and for a delamination from a matrix ply crack in the belt ply in the tapered region. Calculations

for a crack in the thin region correlate reasonably well with the measured failure loads, although they are conservative. Calculations for a crack in the tapered region are slightly more conservative. The calculated values are listed in Table 6.

For the same laminates without interleaf at ABCD, the tested specimens had a variety of failure modes (fig. 13). Delamination onset loads and Gh/N_x^2 values were calculated for a delamination from a matrix crack in the innermost -45 degree dropped ply, with a single adjacent delaminated interface. The thickness and modulus terms were calculated to include the dropped plies; i.e., the total thickness t was equal to 30h and the modulus E_{LAM} was calculated for a $[0_7/(\pm45)_2/0/(\pm45)/0]_s$ laminate. The modulus calculations account for the taper angle of the belt plies in this region. For delamination onset from the dropped ply crack, $Gh/N_x^2 = 65.5 \times 10^{-12}$ in^2/lb. Because these laminates delaminated along GF'D, where there was no interleaf (see fig. 6), calculated failure loads were determined using the DCB data from Table 7 for no interleaf at the delaminating interface. Figure 29 compares the measured onset loads with the calculated onset loads for a laminate with a delamination from a matrix crack in the dropped ply, as shown in fig. 13. The correlation is again very good in this case. Figures 28 and 29 show that not only were the delamination onset lives much longer for the layup B specimens with interleaf than for those without, but the solutions for delamination onset from a matrix crack are also different for the two configurations. It was shown in ref. 9 that under fatigue loading, the presence of the interleaf

material resulted in only a slight improvement in delamination resistance. (See fig. 24.) Therefore, it does not seem likely that the longer failure lives in those specimens are a result of the toughness of the interleaf alone; the improved delamination resistance is more likely due to the additional failure modes when the interleaf is not present (figs. 12, 13). Also, the FE calculations for delamination growth into the tapered region may be conservative because the taper angle in the model is somewhat steeper than the local taper angle at point C in the test specimens.

In refs. 1 and 2, it was assumed that the onset and direction of growth of a delamination was controlled by the magnitude of the peak values of Gh/N_x^2 in figures like figs. 20-22. However, for all the laminate configurations, the Gh/N_x^2 values from the matrix crack solutions were close to or lower than the peak values from the FE analyses for the same configuration, for delamination of the interface between the belt and underlying plies in the tapered region. This would indicate that the delamination would be more likely to fail along ABCD, as shown in fig. 2. However, the FE model for delamination along ABCD does not include matrix cracks, which may change the G calculations for delamination along ABCD. Therefore, a direct comparison of the Gh/N_x^2 values from the two different models was not made.

Calculated delamination onset loads for laminates with matrix cracks proved to correlate fairly well with the measured failure loads for all the IM6/1827I configurations. However, the laminates tested in this study demonstrate that tapered laminates with similar layups and moduli can have very different failure modes. In fact, a variety of failure modes are

possible within a group of laminates of the same configuration. These results indicate that all potential sources for delamination failure, both geometric and material discontinuities, must be considered in order to be able to predict the damage tolerance of tapered composite laminates.

CONCLUSIONS

Tapered laminates of two different layups and two different materials were tested. The materials were S2/SP250 glass/epoxy and IM6/1827I graphite/epoxy. The S2/SP250 material was tested in one layup, $[0_9/(\pm 45)_3/(\pm 45_2)]_s$ (layup A), but in two configurations, with and without a layer of FM73 adhesive at the midplane. The IM6/1827I material was tested in layup A, and in $[0_9/\pm 45/(\pm 45)_3/0/\pm 45/0]_s$ (layup B). Layup B was tested in two configurations, with and without a layer of interleaf material along interface ABCD, that is, between the belt and dropped plies in the tapered region and between the belt and core plies in the thin region. The laminates were loaded in cyclic tension until they delaminated unstably. A finite element analysis showed that for laminates that tended to delaminate along ABCD, the delamination was most likely to start at the junction of the thin and tapered regions and grow in both the thin and tapered regions. However, only the S2/SP250 specimens showed a tendency to fail as modeled in the FE analysis. In these glass/epoxy specimens, calculated strain energy release rate values from the FE model were used with mode I fatigue characterization data from DCB specimens of the test materials to predict delamination onset loads. The IM6/1827I laminates delaminated from matrix ply cracks at a variety of locations. In these laminates, a solution for

the strain energy release rate associated with local delaminations from matrix ply cracks was used to model each observed failure mode. Delamination failure loads were determined using these calculated G values and the mode I fatigue characterization data for IM6/1827I. The following conclusions were reached:

(1) Only the S2/SP250 specimens tended to fail as modeled by the FE analysis. The predicted delamination onset loads using G from the FE analysis were in very good agreement with the experimental values.

(2) For the S2/SP250 laminates, the presence of the adhesive at the midplane had no effect on delamination onset life since the laminates did not fail at the midplane.

(3) All of the IM6/1827I laminates delaminated from matrix cracks. The calculated delamination onset loads using G from the local solution for delamination from matrix ply cracks correlated reasonably well with the experimental values for all configurations when the most commonly observed local delamination was modeled.

(4) The layup B IM6/1827I specimens with interleaf at ABCD exhibited longer delamination onset lives than the same specimens without the interleaf at ABCD. However, the improved delamination resistance was more likely due to the difference in the failure modes of the two configurations than to the enhanced toughness provided by the interleaf.

(5) A variety of different locations for local delamination from matrix ply cracks were observed for the different test configurations. More than one failure mode was also found in specimens of the same configuration. An analysis to predict the damage tolerance of tapered laminates must consider all the possible sources of delamination onset.

REFERENCES

[1] Salpekar, S.A., Raju, I.S., and O'Brien, T.K., "Strain Energy Release Rate Analysis of Delamination in Tapered Laminate Subjected to Tension Load," NASA TM-102592, March 1990.

[2] Murri, G.B., Salpekar, S.A., and O'Brien, T.K., "Fatigue Delamination Onset Prediction in Unidirectional Tapered Laminates," Presented at the ASTM 3rd Symposium on Composite Materials: Fatigue and Fracture, Orlando, FL, November, 1989.

[3] Chan, W.S., Rogers, C., and Aker, S., "Improvement of Edge Delamination Strength of Composite Laminates Using Adhesive Layers," Composite Materials: Testing and Design, ASTM STP 893, J. M. Whitney, Ed., American Society for Testing and Materials, Philadelphia, 1986, p.266-285.

[4] Rybicki, E. F., and Kanninen, M. F., "A Finite Element Calculation of Stress-Intensity Factors by a Modified Crack-Closure Integral," Engineering Fracture Mechanics, Vol. 9, 1977, pp. 931-938.

[5] O'Brien, T.K., "Analysis of Local Delaminations and Their Influence on Composite Laminate Behavior," Delamination and Debonding of Materials, ASTM STP 876, W. S. Johnson, Ed., American Society for Testing and

Materials, Philadelphia, PA, 1985, pp. 282-297.

[6] O'Brien, T. K., Rigamonti, M. and Zanotti, C., "Tension fatigue analysis and life prediction for composite laminates," Int. Journal of Fatigue, Vol. 11, No. 6, pp. 379-393.

[7] Salpekar, S. A., and O'Brien, T. K., "Combined Effect of Matrix Cracking and Free Edge on Delamination," NASA TM-102591, March 1990.

[8] Shivakumar, K. N., and Crews, J. H., "Bolt Clampup Relaxation in a Graphite/Epoxy Laminate," Long Term Behavior of Composites, ASTM STP 813, T. K. O'Brien, Ed., American Society for Testing and Materials, Philadelphia, 1983, pp. 5-22.

[9] Martin, R.H., "Characterizing Fatigue Delamination of Composite Materials Using the Double Cantilever Beam Specimen," NASA CR-181991, 1990.

[10] O'Brien, T. K., "Mixed-Mode Strain-Energy-Release Rate Effects on Edge Delamination of Composites," Effects of Defects in Composite Materials ASTM STP 836, American Society for Testing and Materials, 1984, pp. 125-142.

[11] Adams, D. F., Zimmerman, R. S., and Odom, E. M., "Frequency and Load Ratio Effects on Critical Strain Energy Release Rate G_c Thresholds of Graphite/Epoxy Composites," Toughened Composites, ASTM STP 937, Norman

J. Johnston, Ed., American Society for Testing and Materials, Philadelphia, 1987, pp. 242-259.

[12] Martin, R. H., and Murri, G. B., "Characterization of Mode I and Mode II Delamination Growth and Thresholds in Graphite/PEEK Composites," NASA TM-100577, April 1988.

Table 1. Specimen configurations and failure modes.

Material	Layup	Total No. of Test Specimens	Failure Mode	No. of Specimens with given failure
S2/SP250	A	18	9(a)	10
			9(b)	2
			9(c)	2
IM6/1827I	A	13	10(a)	7
			10(b)	4
			10(c)	2
IM6/1827I	B with interleaf	8	12(a)	4
			12(b)	4
IM6/1827I	B without interleaf	8	13(a)	2
			13(a) and 13(b)	4
			12(a)	2

Table 2. Material Properties[8]

	S2/SP250	IM6/1827I	Neat Resin[7]
$E_{11} \times 10^6$ psi	6.600	19.000	0.595
$E_{22} \times 10^6$ psi	2.100	0.856	0.595
$G_{12} \times 10^6$ psi	0.880	0.615	0.224
ν_{12}	0.275	0.361	0.330
V_f, %	57.0	53.5	----

Table 3. Longitudinal moduli of thin and thick regions in tapered laminates

	E_{xx} x 10^6 psi	E_{LPT} x 10^6 psi	h, in.	V_f, %
S2/SP250				
no adhesive at midplane				
Thin	6.130	5.40	0.0083	58.7
Thick	4.690	4.53	0.0083	56.5
S2/SP250				
adhesive at midplane				
Thin	5.470	5.40	0.0085	57.3
Thick	4.540	4.53	0.0084	55.5
IM6/1827I				
Layup A				
Thin	13.87	13.91	0.0080	54.7
Thick	10.28	10.22	0.0081	52.7
IM6/1827I				
Layup B				
Thin	14.29	13.91	0.0080	54.7
Thick	10.17	10.22	0.0081	52.7

Table 4. S2/SP250 glass/epoxy, layup A.

G-N data (DCB tests)		calculated delamination onset loads P_{max}(N) from FE model, lbs	
G_{Imax}, in-lb/in^2	N, cycles	thin region*	tapered region**
0.085	1,066,500	8,627	7,253
0.192	14,610	12,966	10,901
0.277	2,510	15,574	13,093
0.185	92,090	12,728	10,700
0.332	1,200	17,051	14,334
0.085	521,090	8,627	7,253
0.124	466,250	10,420	8,725
0.203	97,490	13,333	11,208
0.216	2,700	13,753	11,562
0.119	303,820	10,208	8,582
0.493	1,000	20,778	17,467
0.085	2,000,000	8,627	7,253

* $\left(\frac{Gh}{N_x^2}\right)_{FE} = 37.00 \times 10^{-12} \frac{\text{in-lb}}{\text{in}^2}$ ** $\left(\frac{Gh}{N_x^2}\right)_{FE} = 52.57 \times 10^{-12} \frac{\text{in-lb}}{\text{in}^2}$

Table 5. IM6/1827I graphite/epoxy, layup A.

G-N data (DCB tests) with interleaf		calculated delamination onset loads, lbs		
G_{Imax}, in-lb/in^2	N, cycles	matrix crack in core ply		matrix crack in dropped ply
		thin region	tapered region	
1.417	7,440	27,561	22,919	22,077
0.800	41,150	20,709	17,221	16,588
0.509	1,015,480	16,518	13,736	13,231
1.417	36,840	27,561	22,919	22,077
0.794	78,730	20,631	17,156	16,526
0.510	415,650	16,535	13,750	13,244
0.754	30,260	20,105	16,719	16,104
1.420	21,000	27,590	22,934	22,100
1.370	38,410	27,100	22,536	21,707
0.777	65,570	20,409	16,972	16,348

Table 6. IM6/1827I graphite/epoxy, layup B with interleaf at ABCD.

G-N data (DCB tests) with interleaf		calculated delamination onset loads, lbs	
G_{Imax}, in-lb/in^2	N, cycles	matrix crack in belt ply	
		thin region	tapered region
1.417	7,440	29,701	24,549
0.800	41,150	22,317	18,446
0.509	1,015,480	17,801	14,713
1.417	36,840	29,701	24,549
0.794	78,730	22,233	18,376
0.510	415,650	17,819	14,728
0.754	30,260	21,666	17,908
1.420	21,000	29,733	24,575
1.370	38,410	29,205	24,139
0.777	65,570	21,994	18,179

Table 7. IM6/1827I graphite/epoxy, layup B without interleaf at ABCD.

G-N data (DCB tests) without interleaf		calculated delamination onset loads, lbs
G_{Imax}, in-lb/in^2	N, cycles	matrix crack in dropped ply
0.525	31,510	16,110
0.813	22,250	20,048
0.334	515,110	12,850
0.759	17,870	19,370
0.216	269,030	10,330
0.507	366,870	15,832
0.793	10,930	19,800
0.477	138,170	15,356
0.477	458,400	15,356

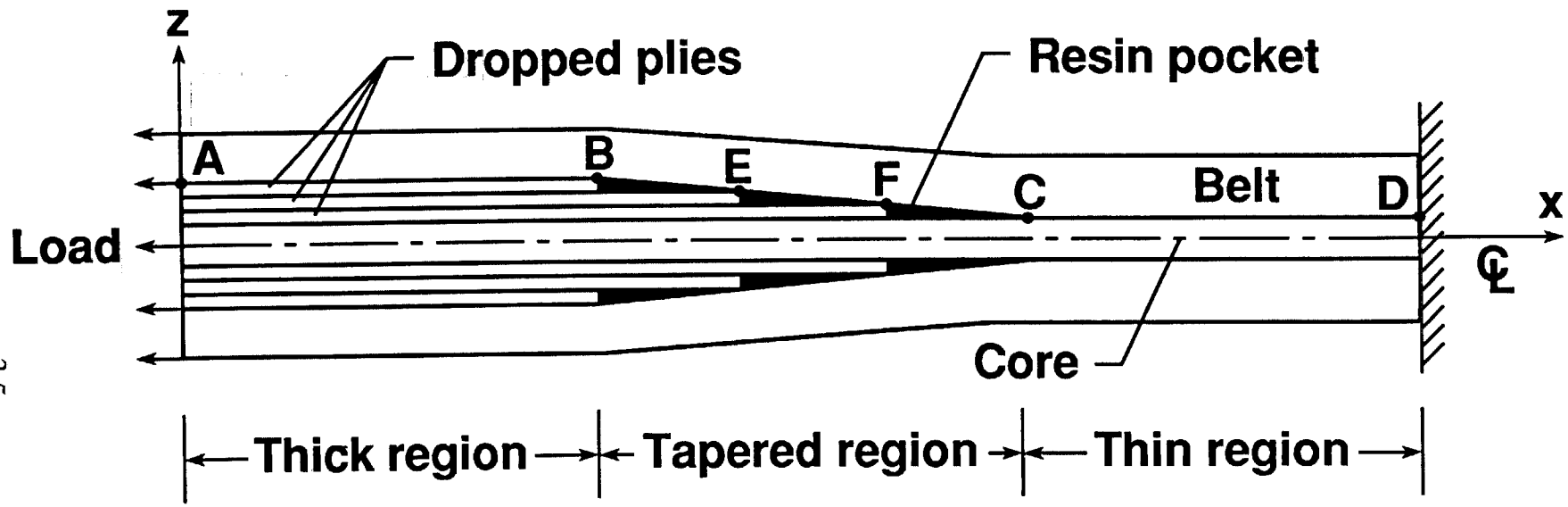

Figure 1. Tapered laminate configuration and loading.

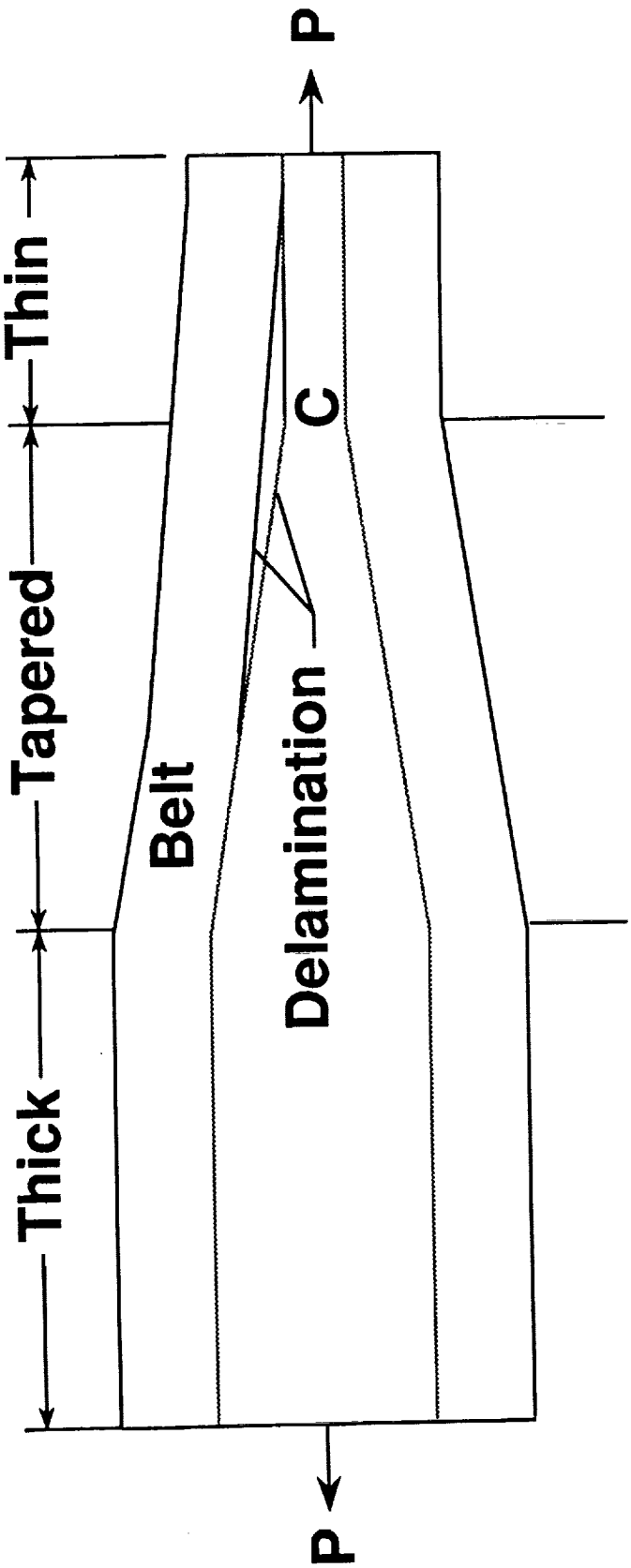

Figure 2. Delamination growth in tapered laminates.

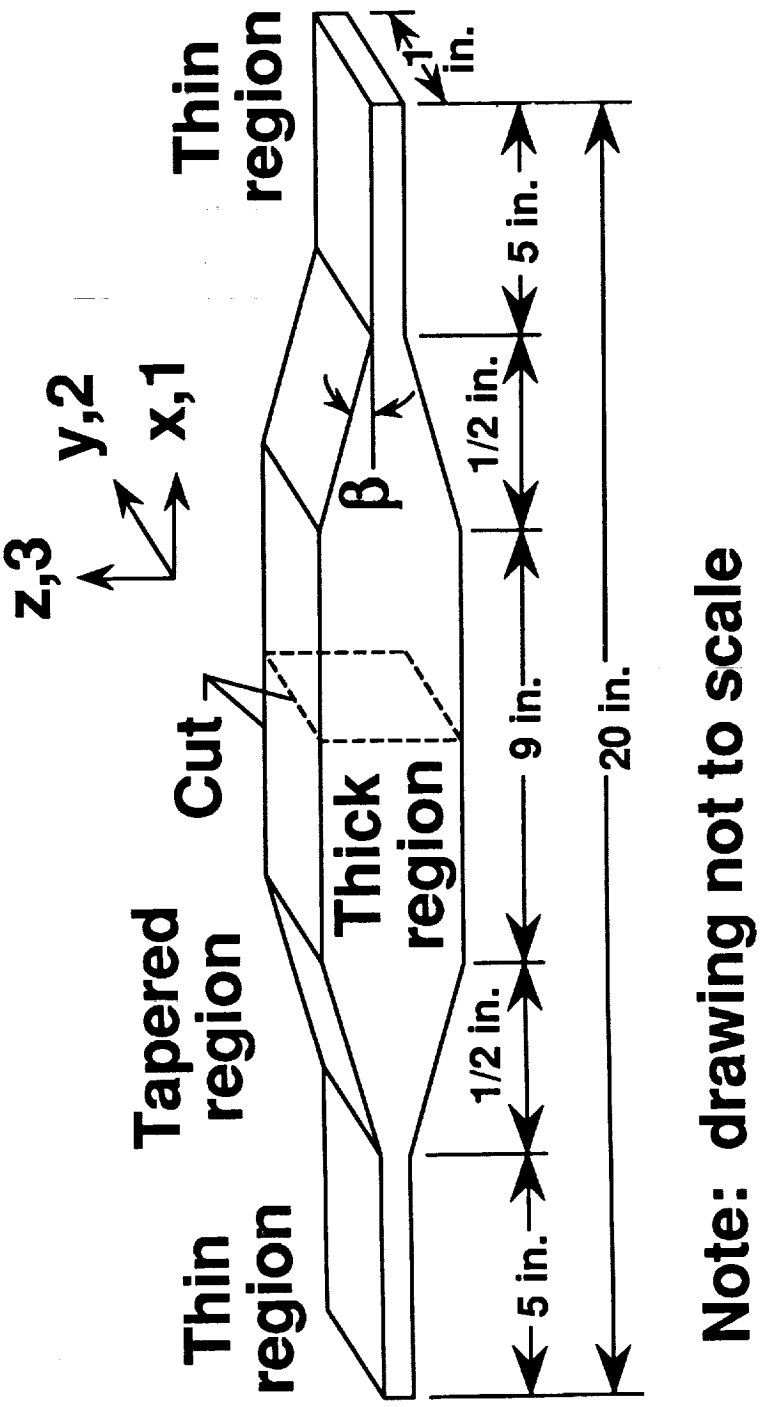

Figure 3. Laminates cut from tapered panels.

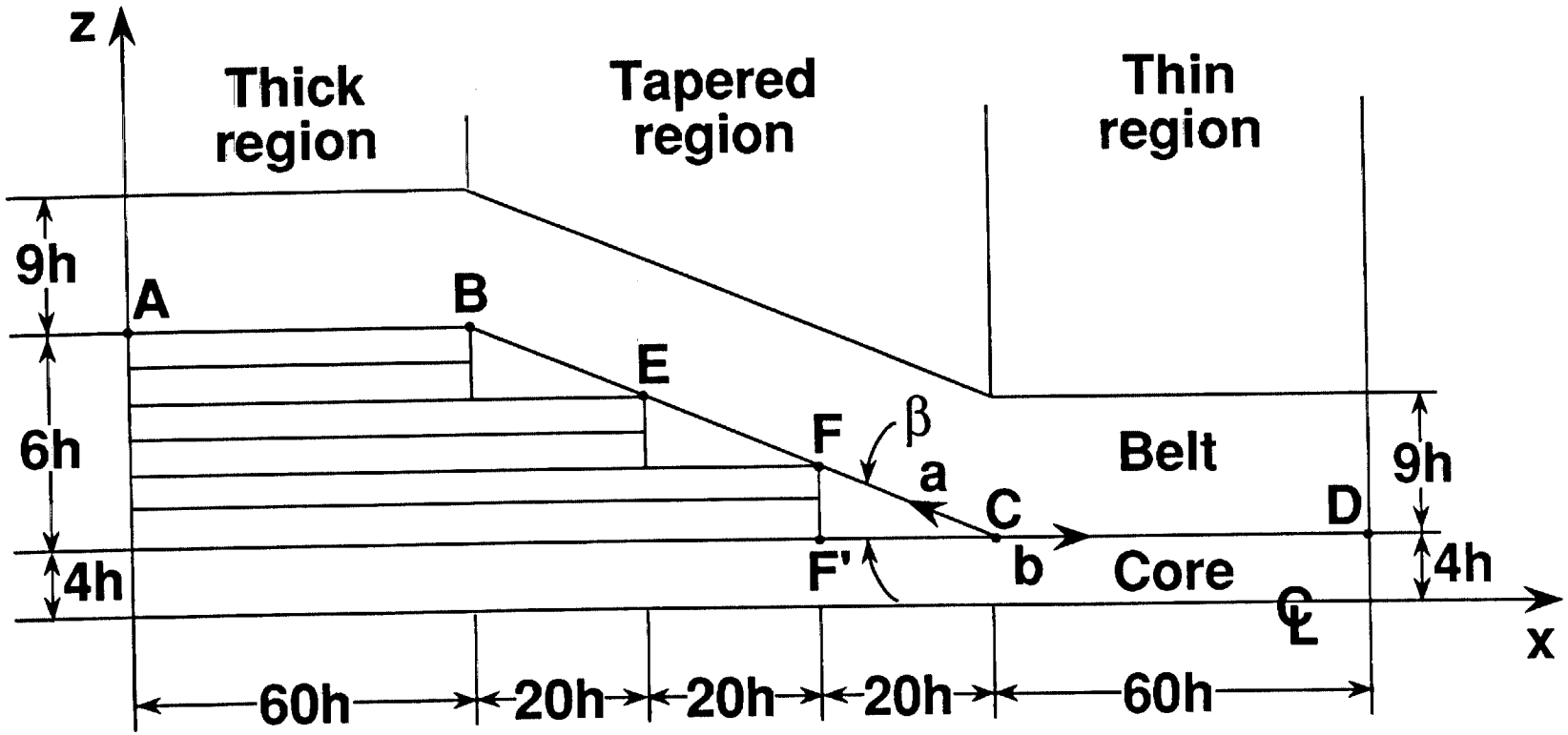

Figure 4. Tapered laminate with internal ply drops.

Figure 5. Dropped ply locations in IM6/1827I layup A laminate.

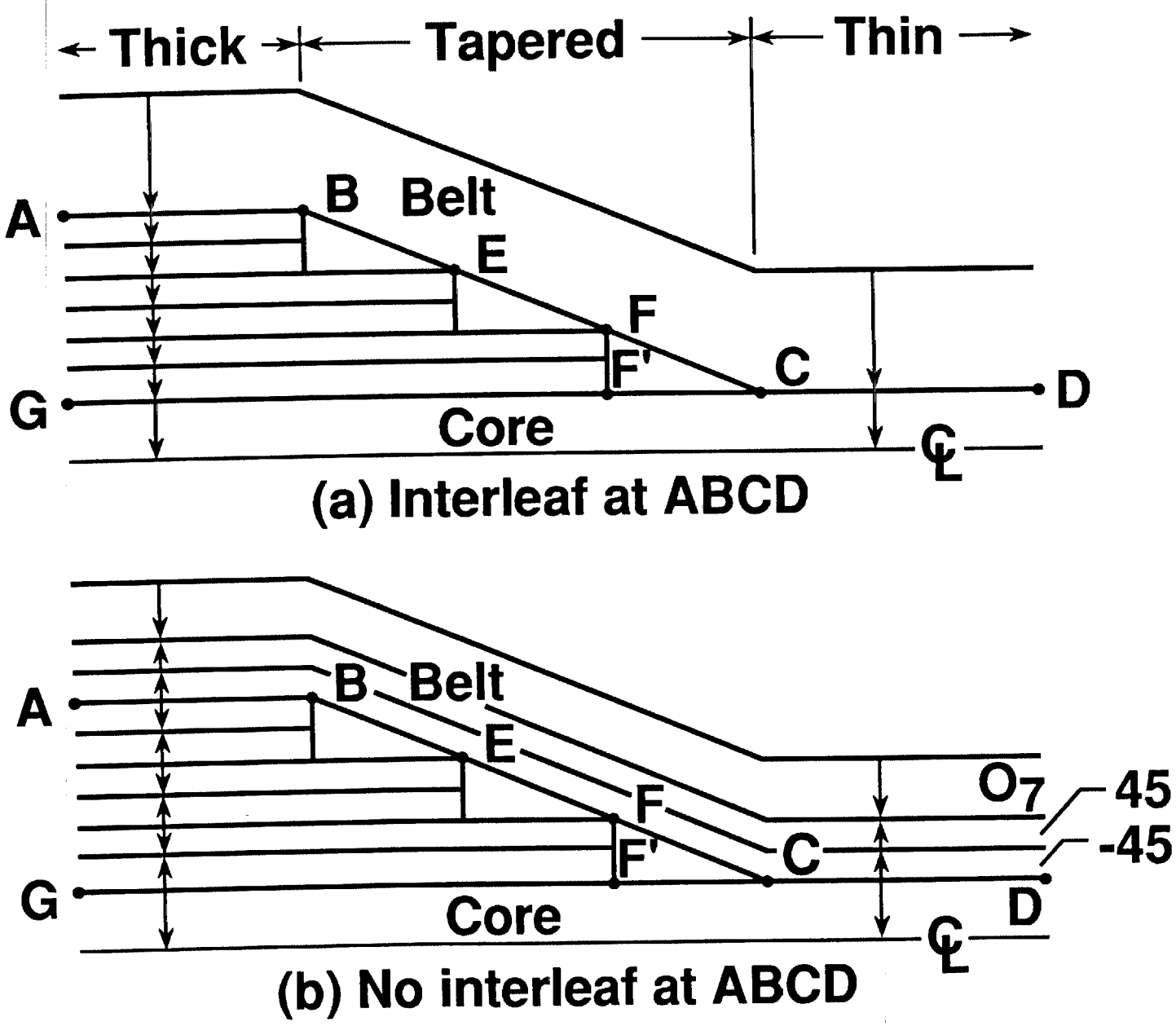

Figure 6. Interleaf locations in IM6/1827I layup B laminates.

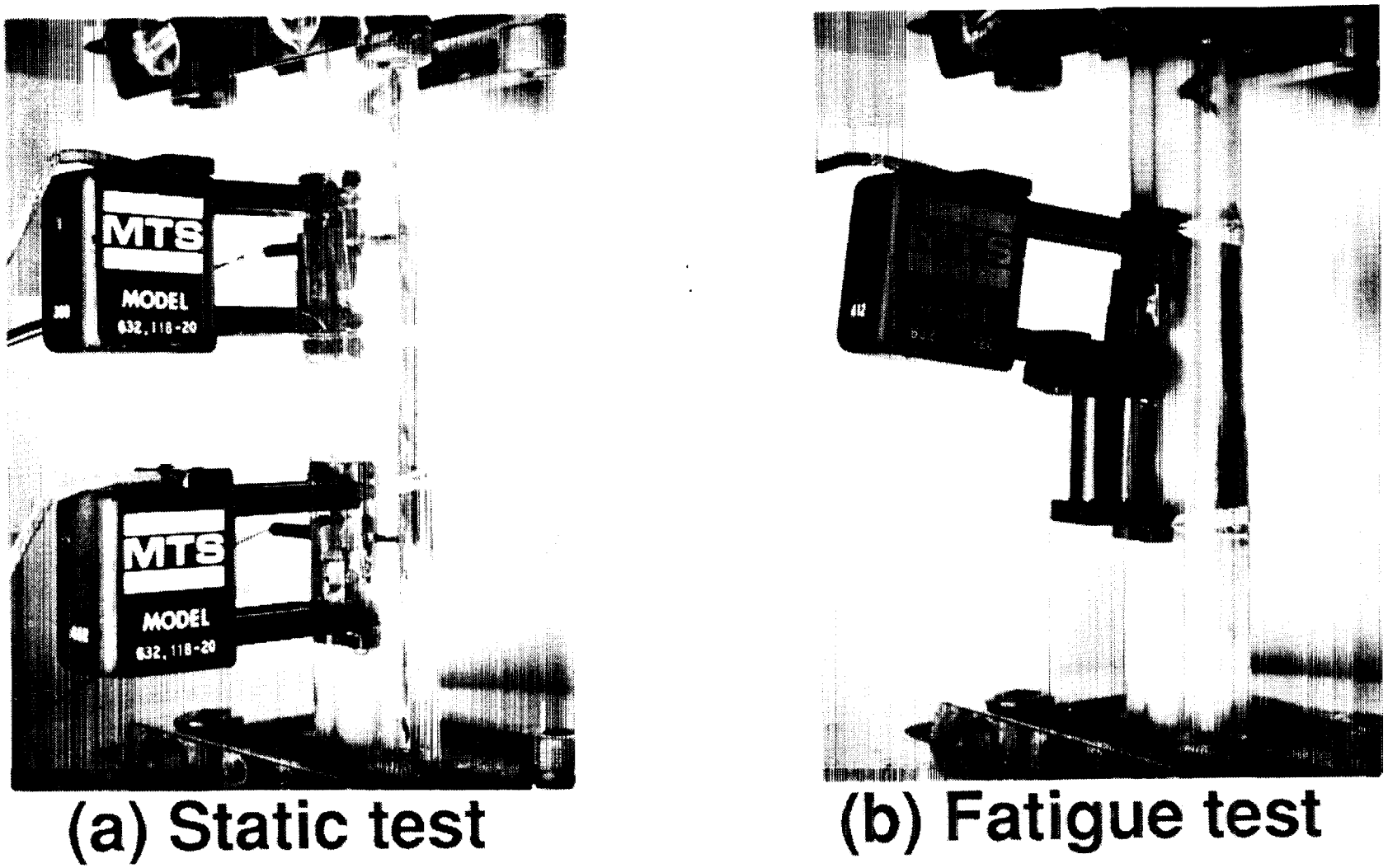

Figure 7. Photographs of test specimens in hydraulic load frame with mounted extensometers.

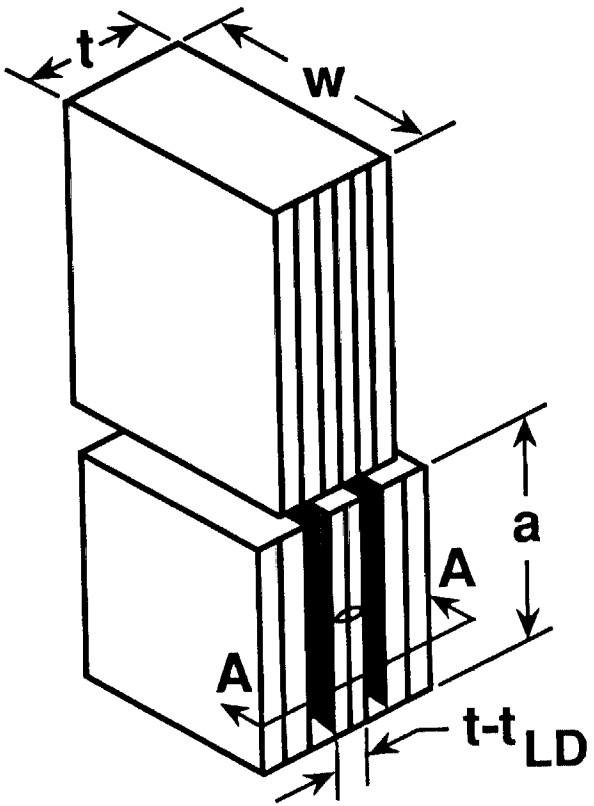

(a) Model of local delamination[5]

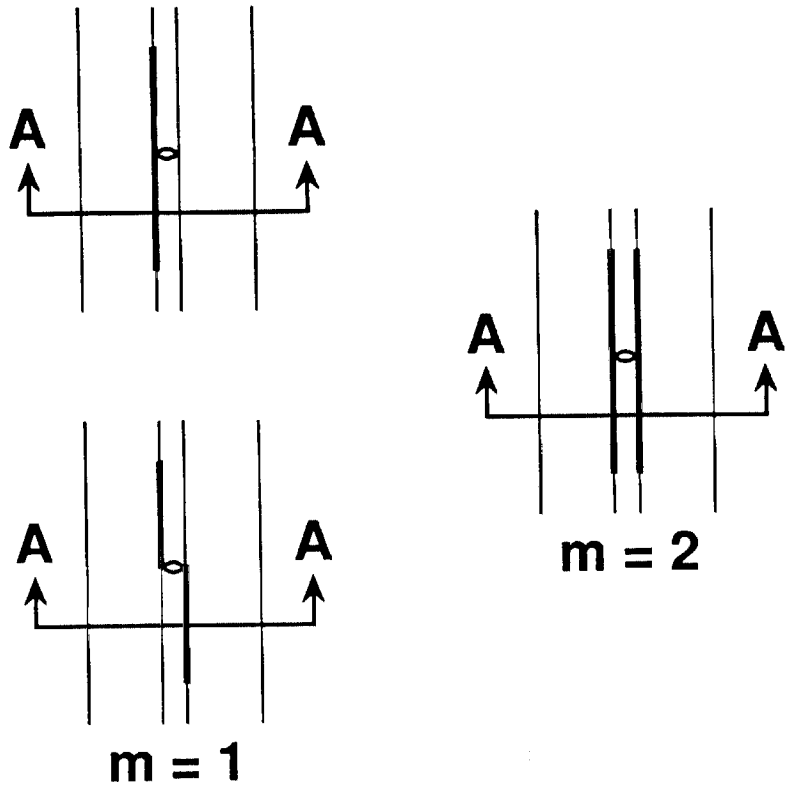

(b) Number m of delamination planes growing from matrix ply crack

Figure 8. Matrix ply cracks and associated local delaminations.

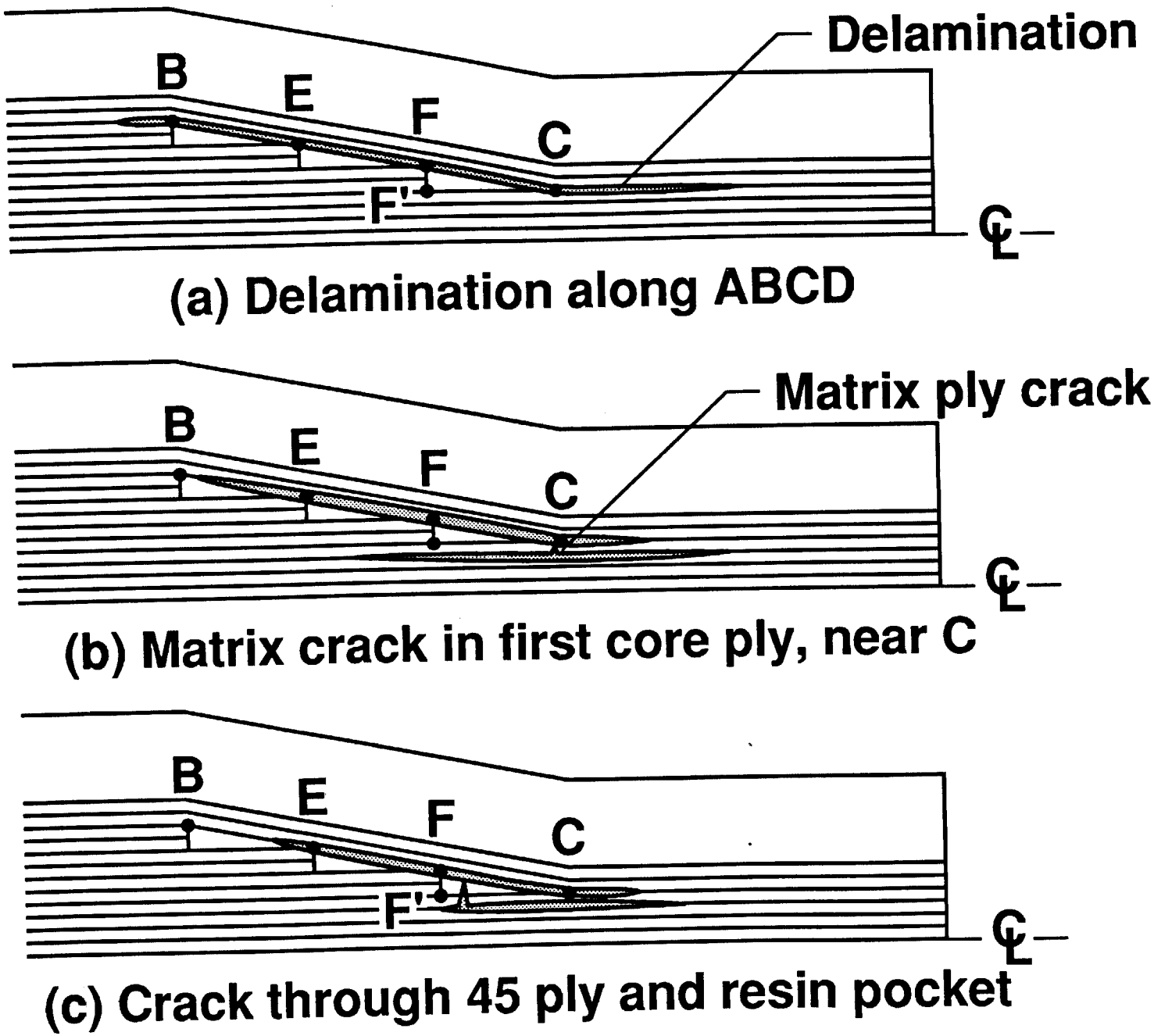

Figure 9. Delamination damage in S2/SP250 laminates.

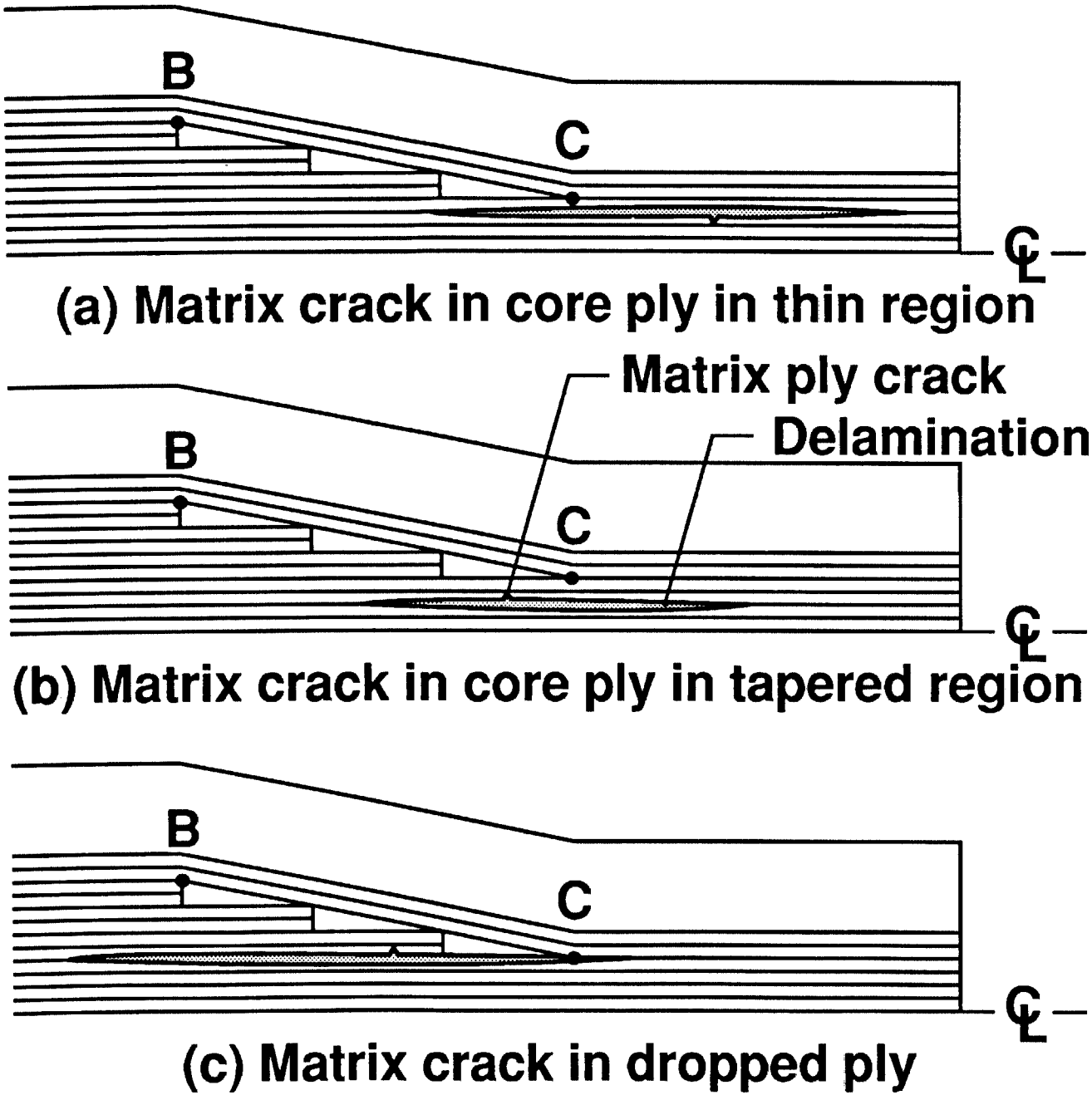

Figure 10. Delamination damage in IM6/1827I layup A laminates.

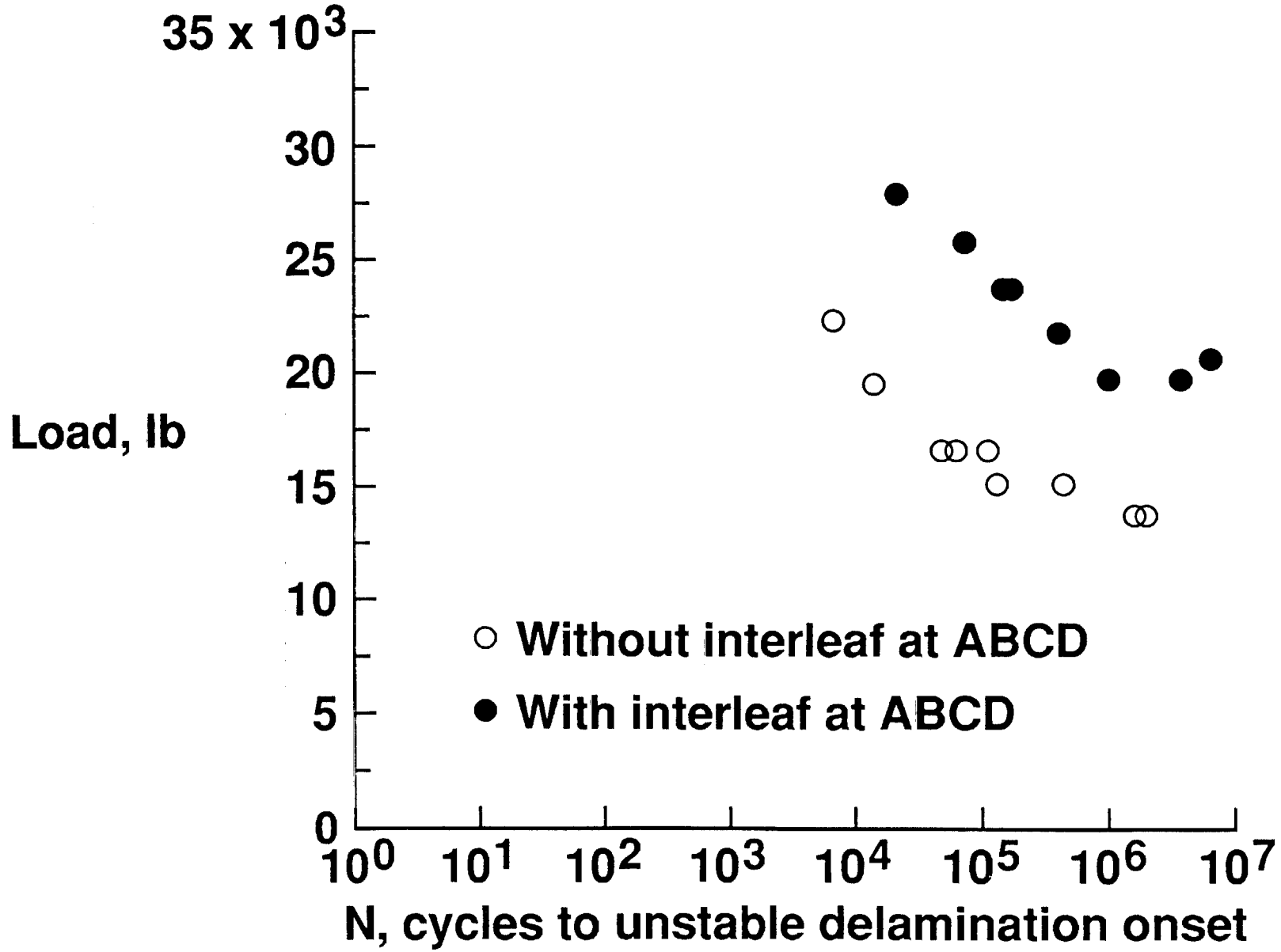

Figure 11. Experimental results for IM6/1827I layup B laminates.

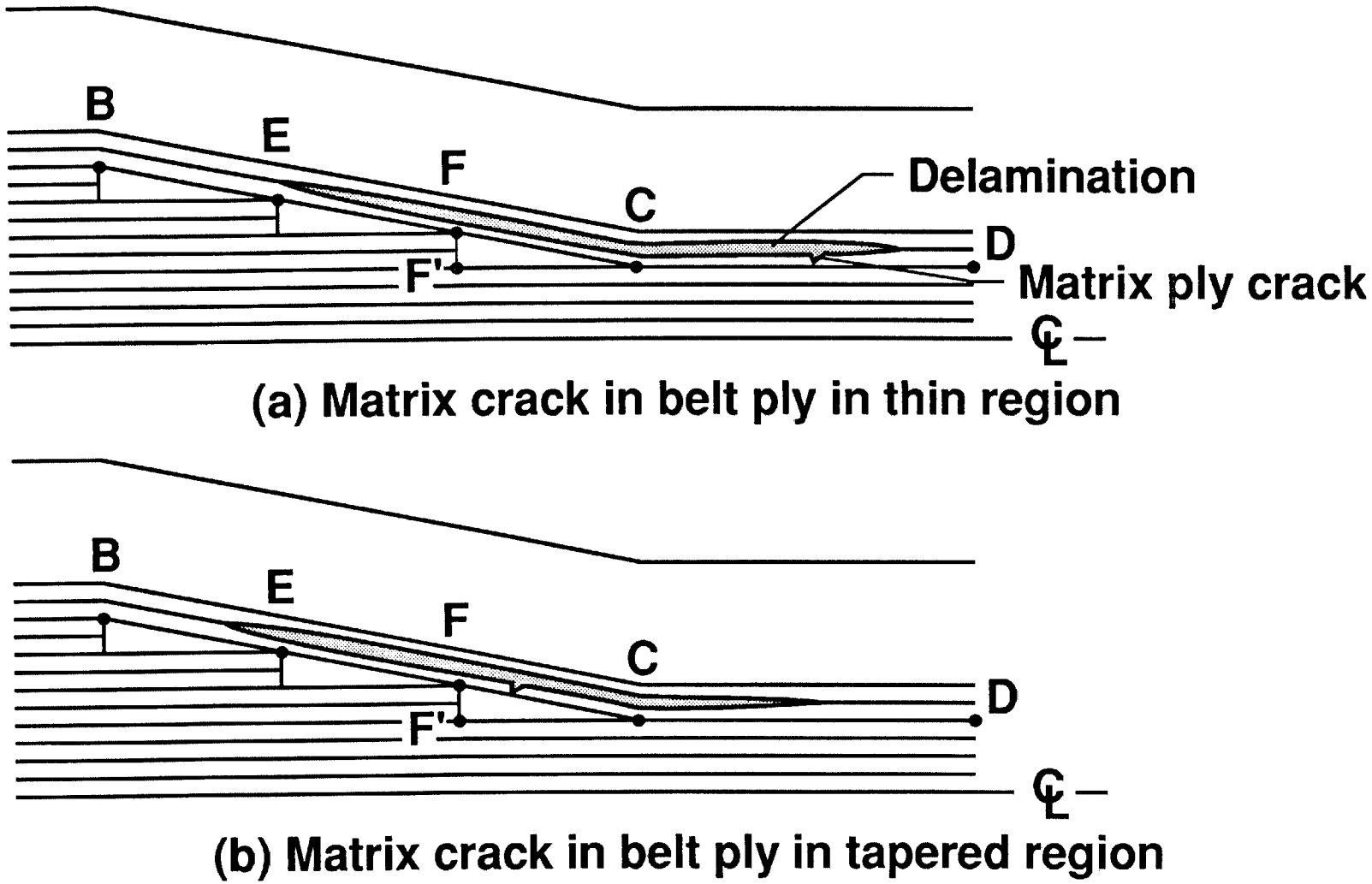

Figure 12. Delamination damage in IM6/1827I layup B laminates with interleaf at ABCD.

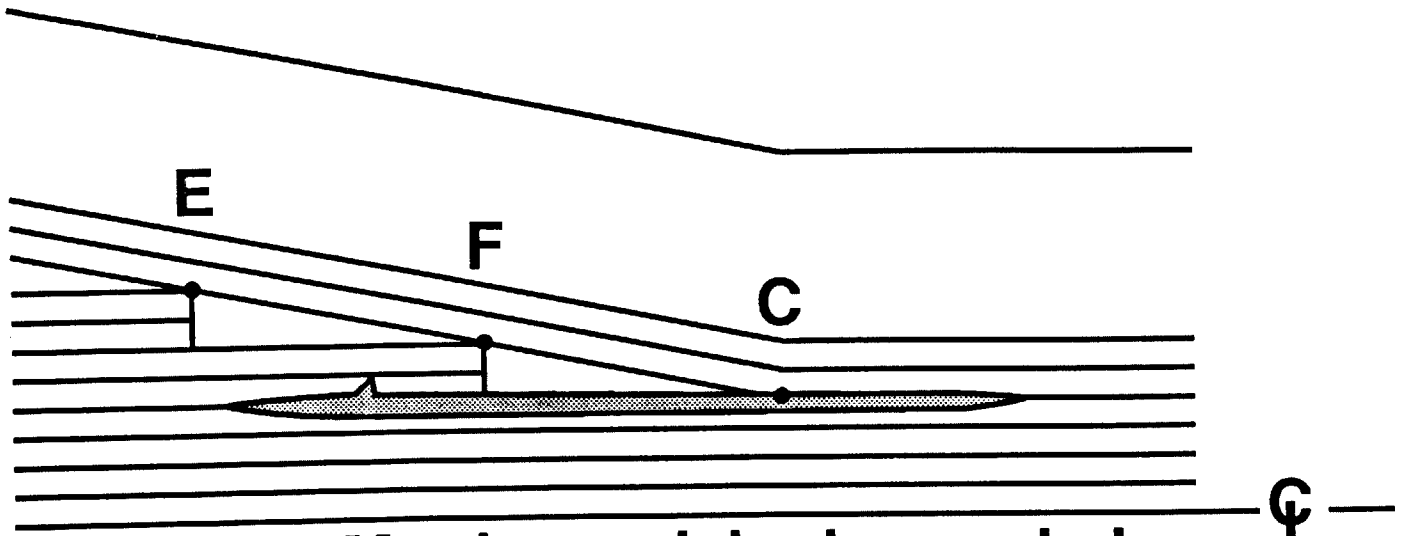

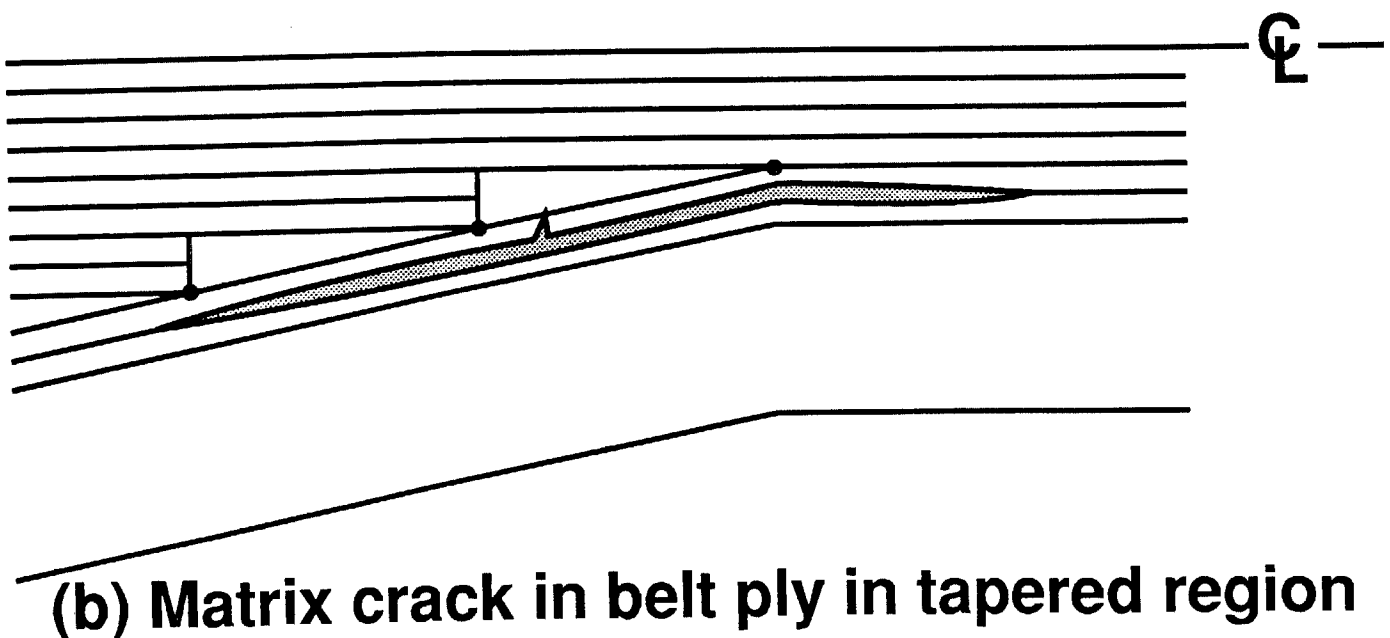

Figure 13. Delamination damage in IM6/1827I layup B laminates without interleaf at ABCD.

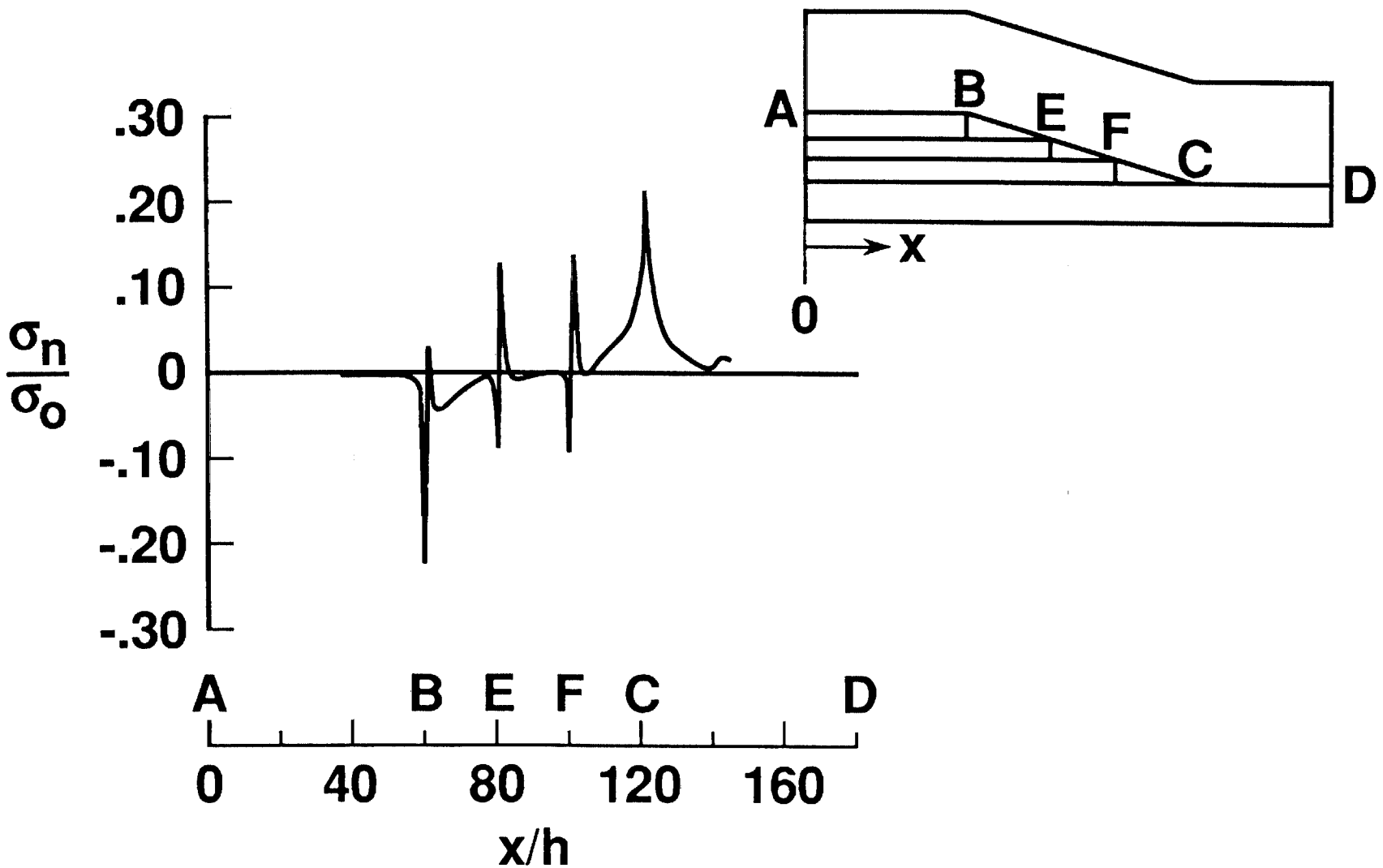

Figure 14. Interlaminar normal stress in S2/SP250 layup A laminates.

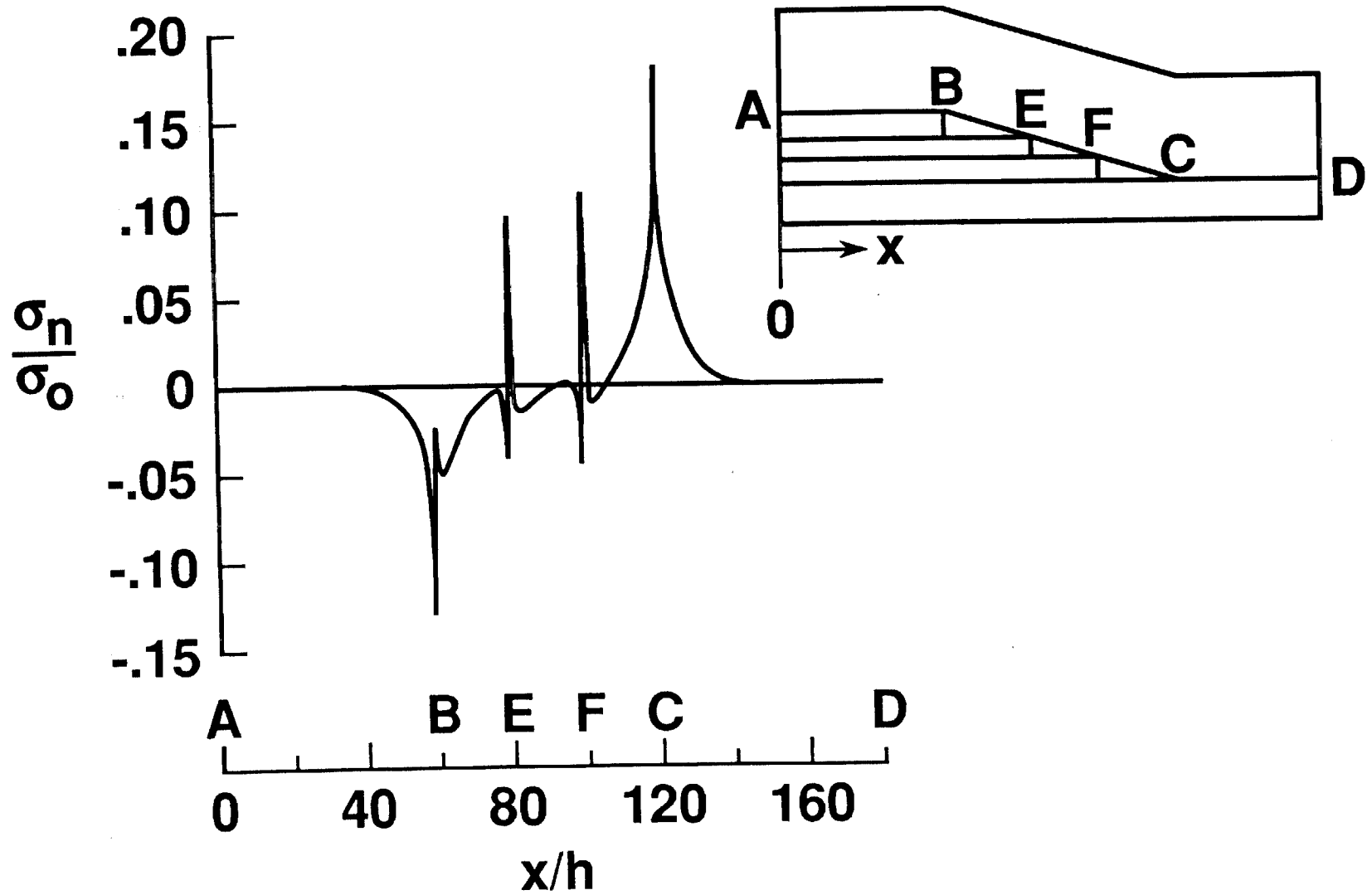

Figure 15. Interlaminar normal stress in IM6/1827I layup A laminates.

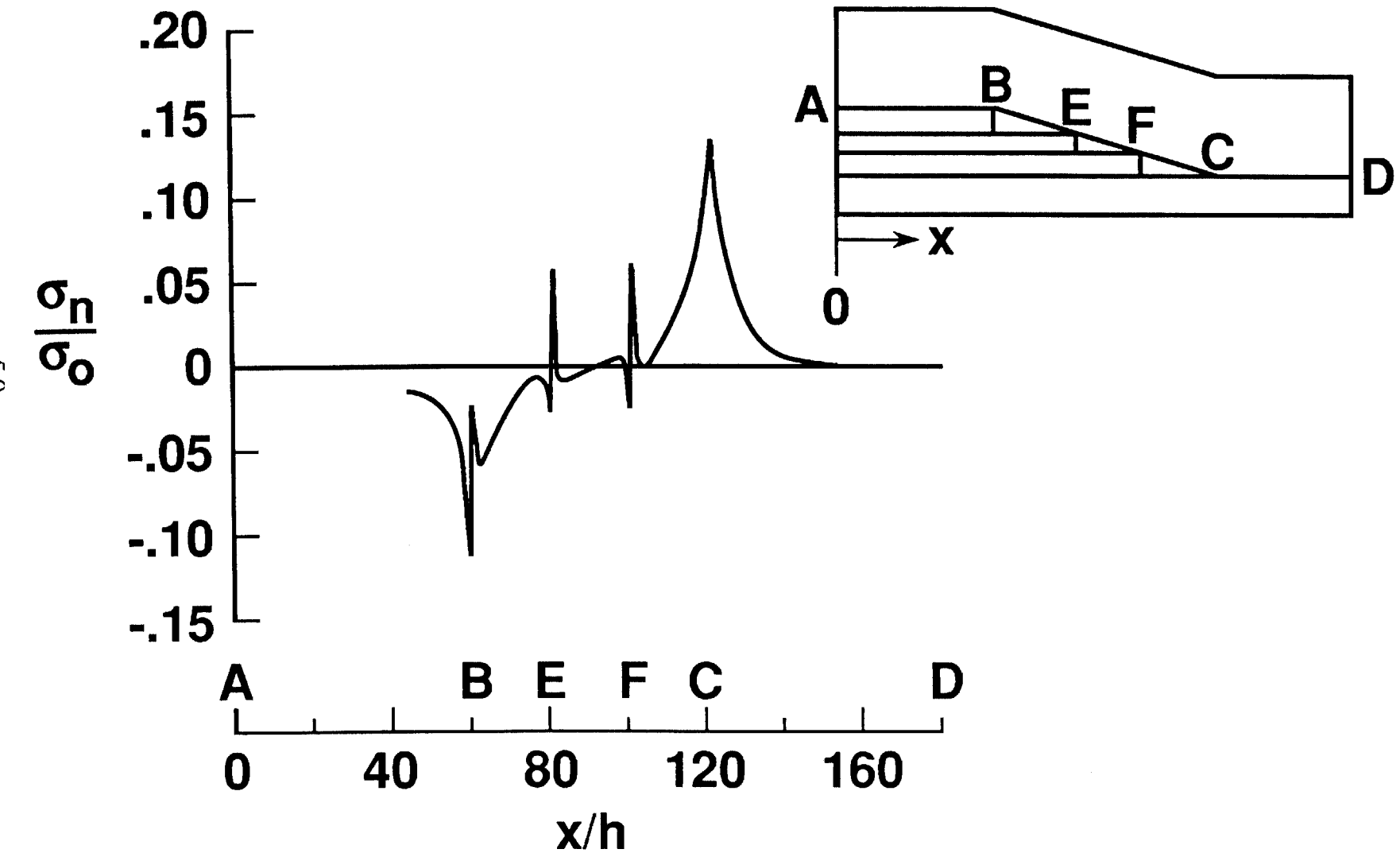

Figure 16. Interlaminar normal stress in IM6/1827I layup B laminates.

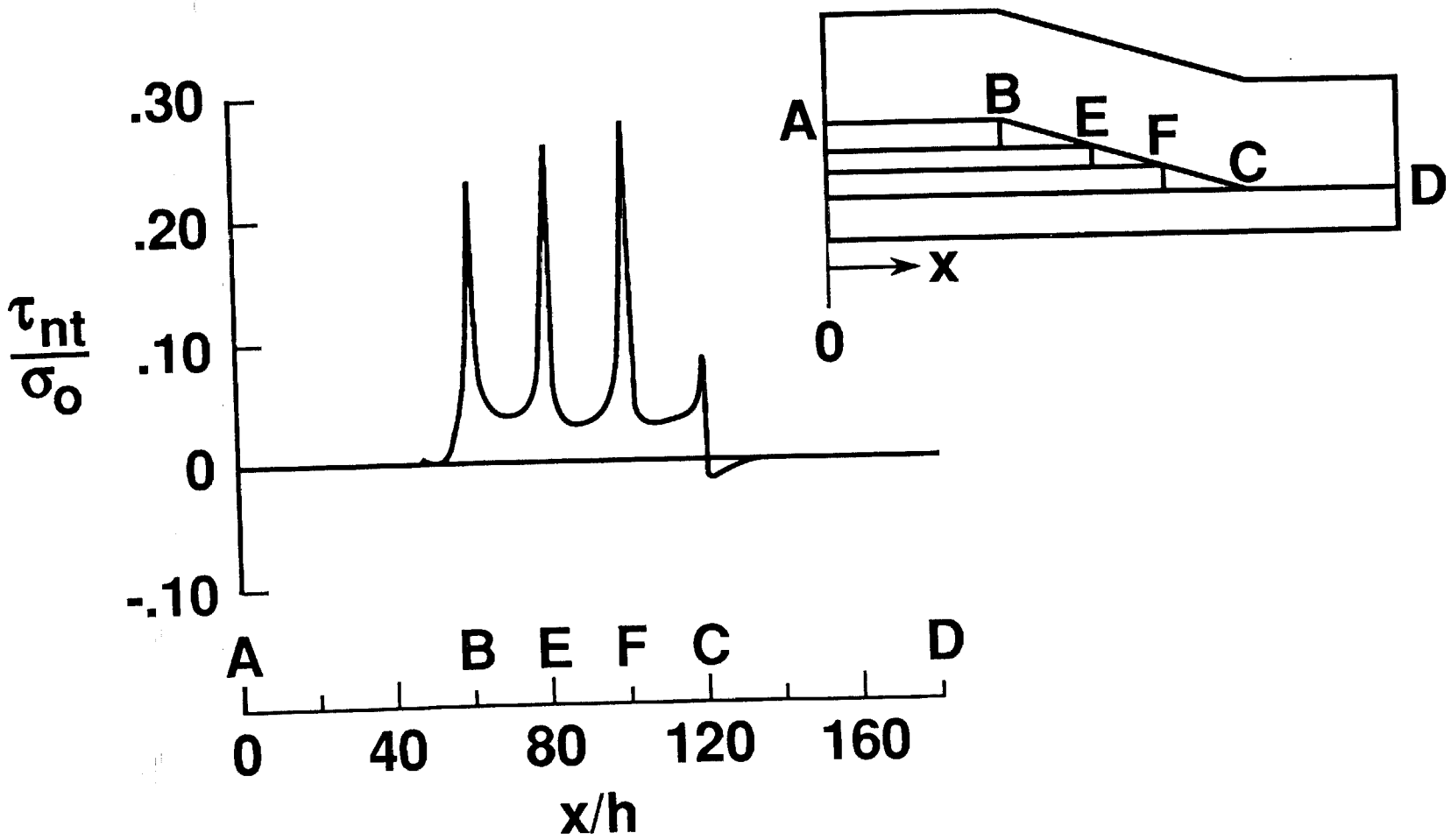

Figure 17. Interlaminar shear stress in S2/SP250 layup A laminates.

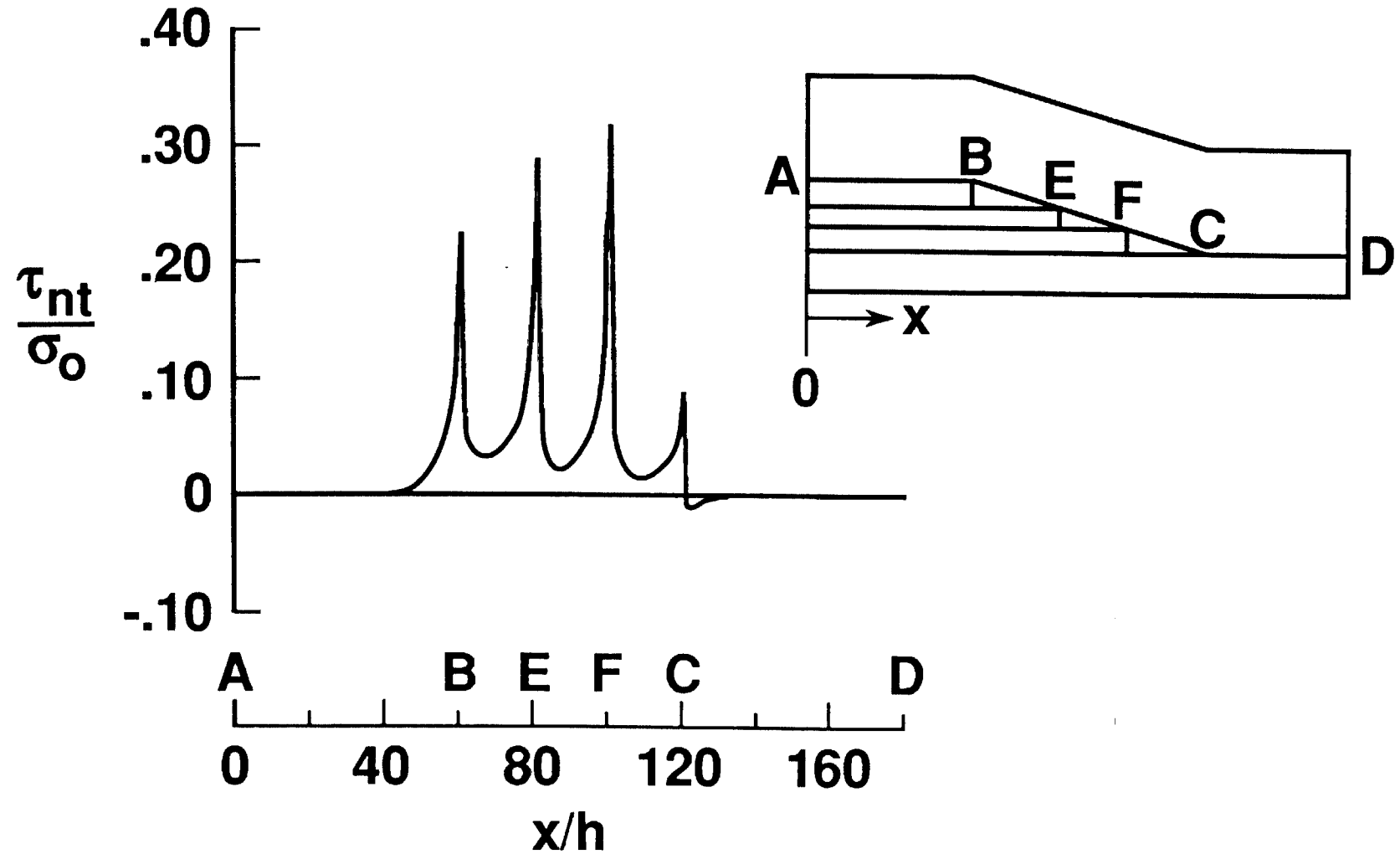

Figure 18. Interlaminar shear stress in IM6/1827I layup A laminates.

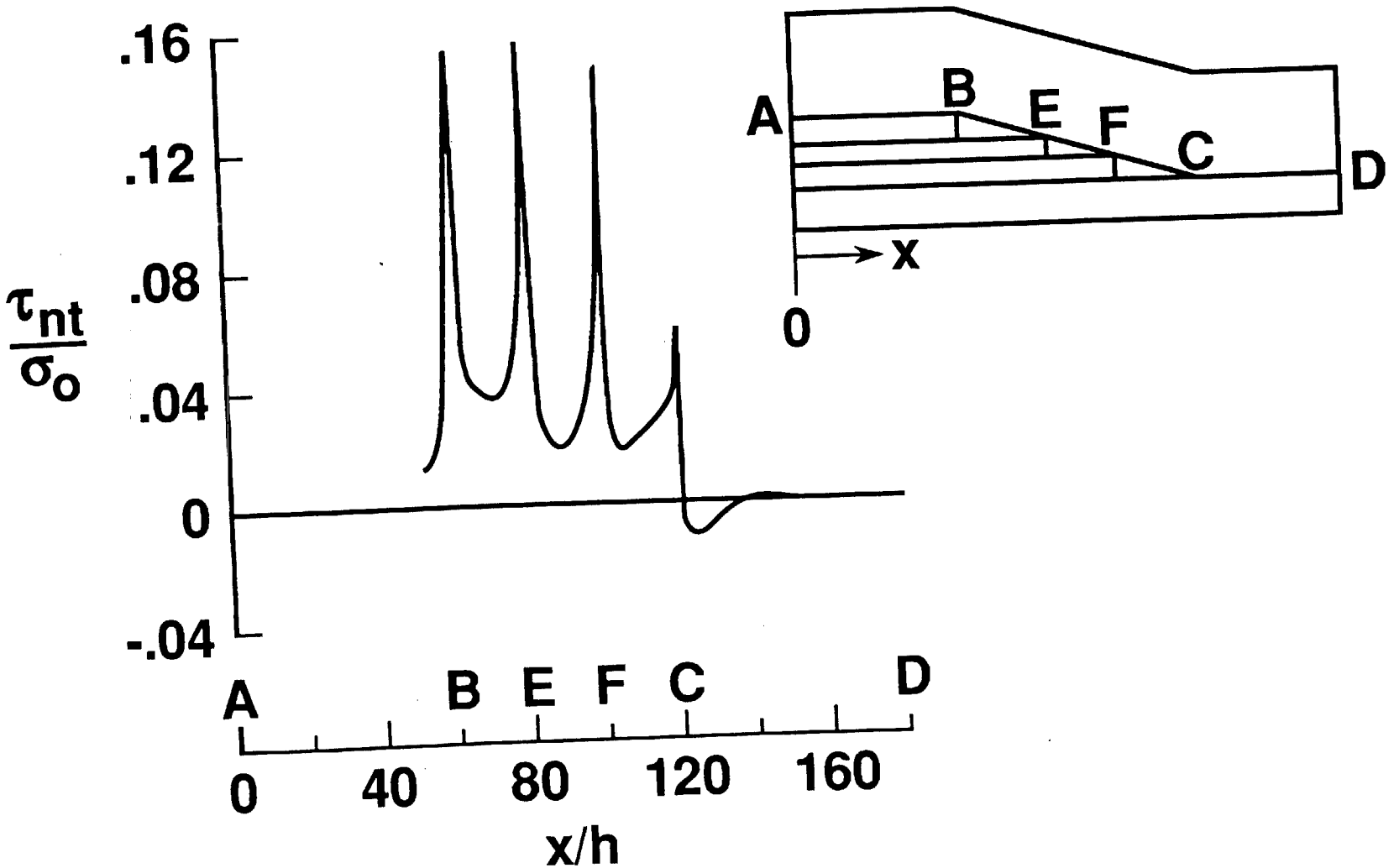

Figure 19. Interlaminar shear stress in IM6/1827I layup B laminates.

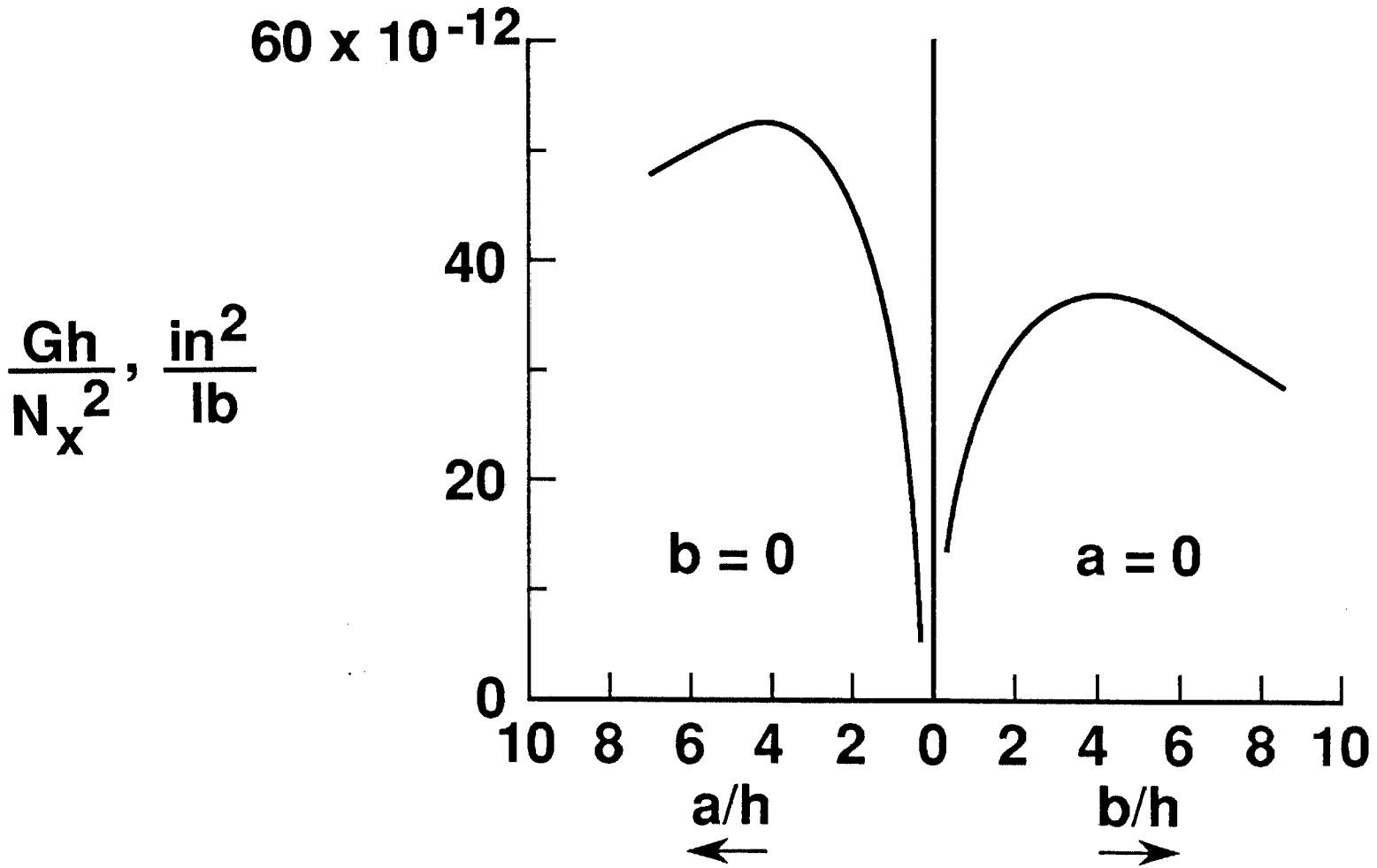

Figure 20. Normalized strain energy release rates in S2/SP250 layup A laminates.

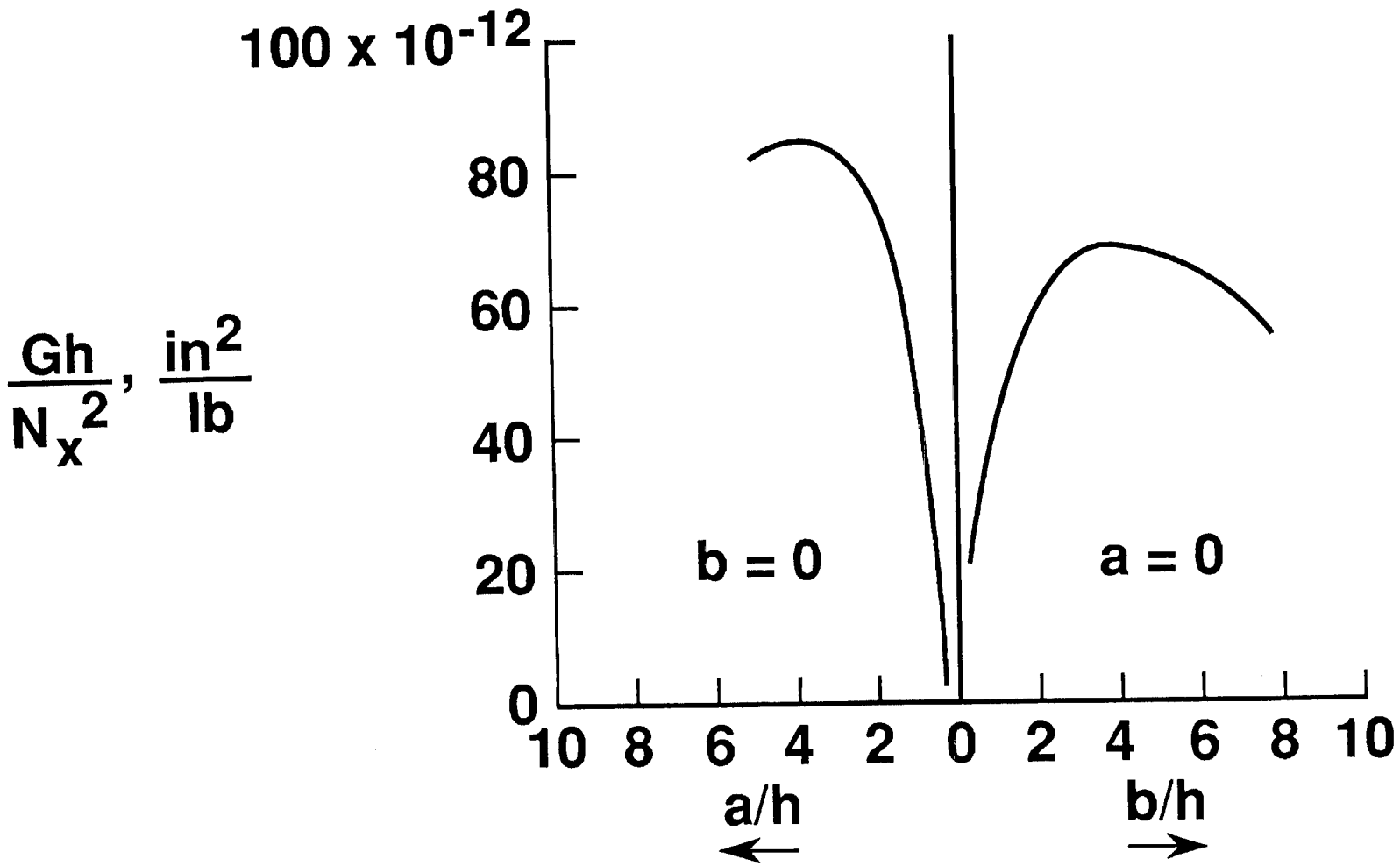

Figure 21. Normalized strain energy release rates in IM6/1827I layup A laminates.

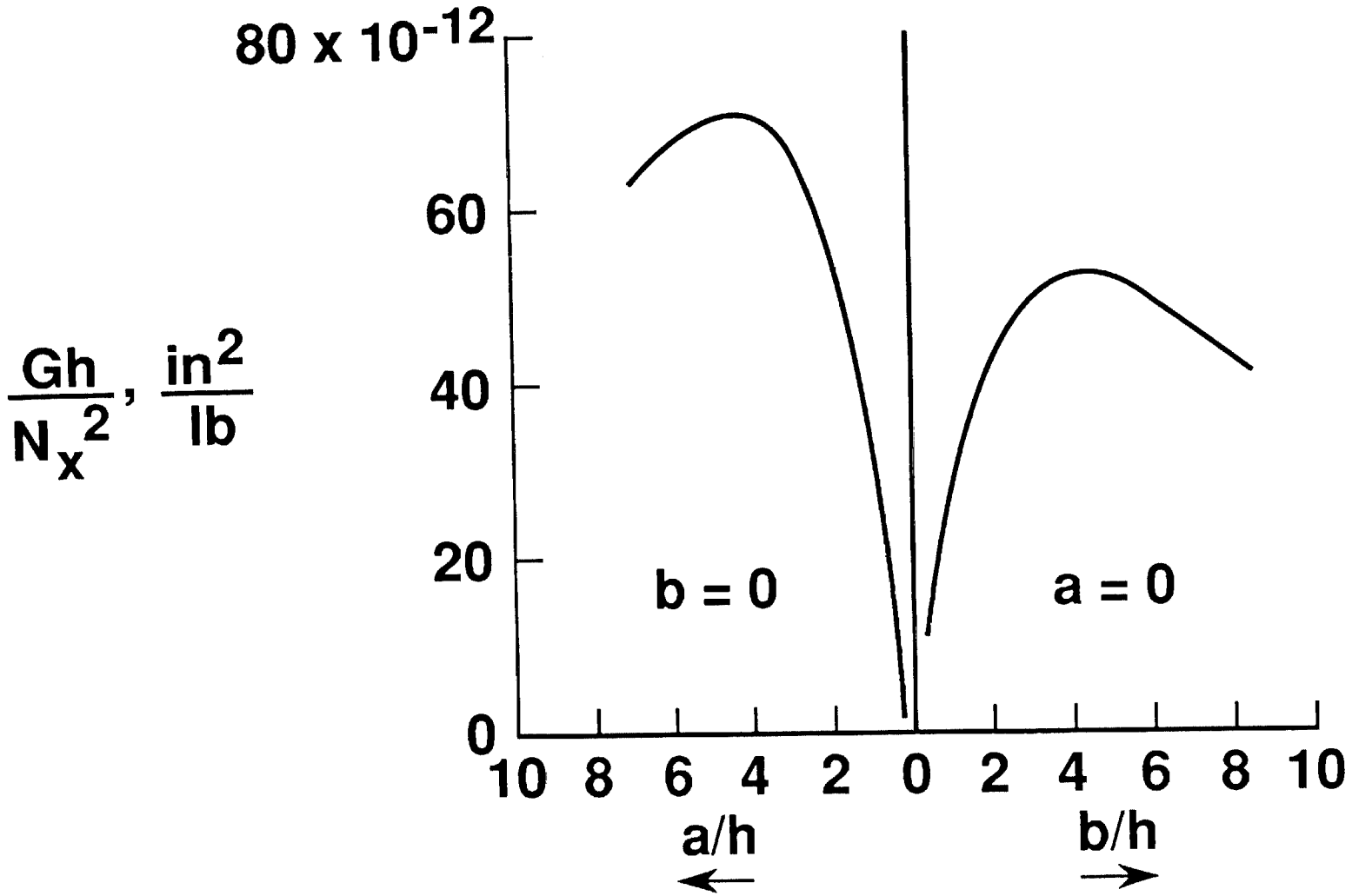

Figure 22. Normalized strain energy release rates in IM6/1827I layup B laminates.

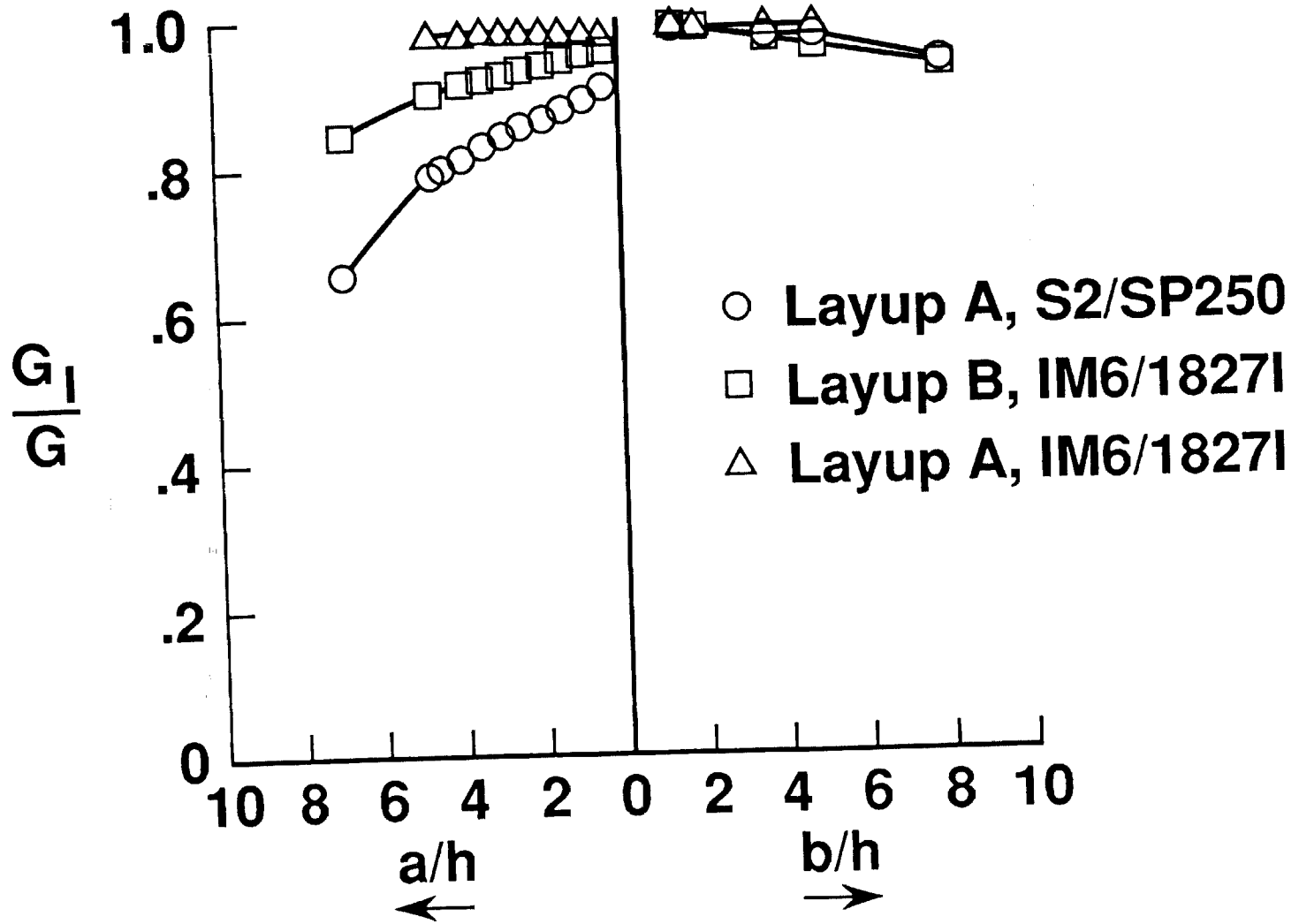

Figure 23. Ratio of G_I to total G for delamination growth in tapered laminates.

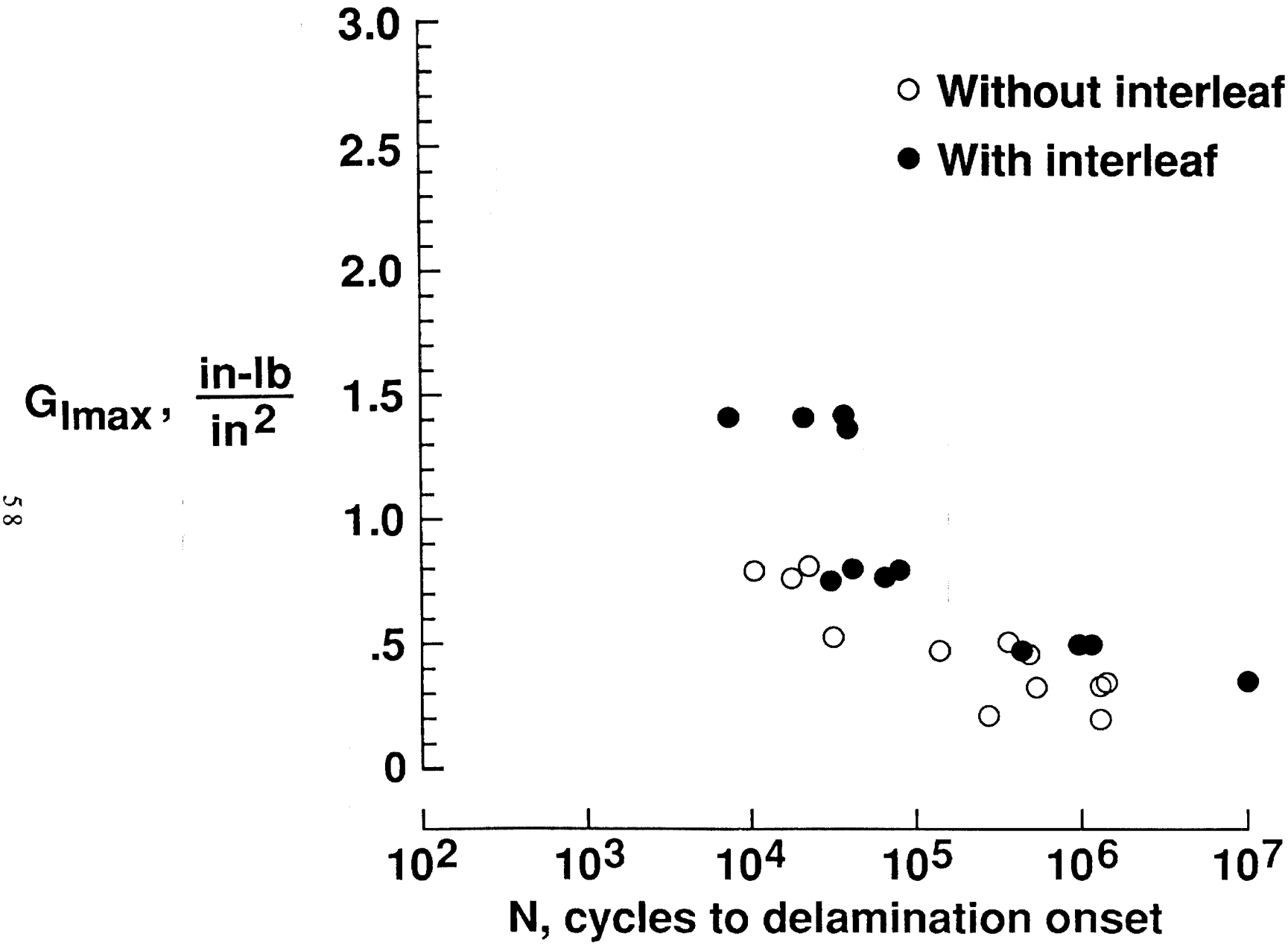

Figure 24. G_{Imax} as a function of cycles to delamination onset for IM6/1827I material, with and without interleaf.

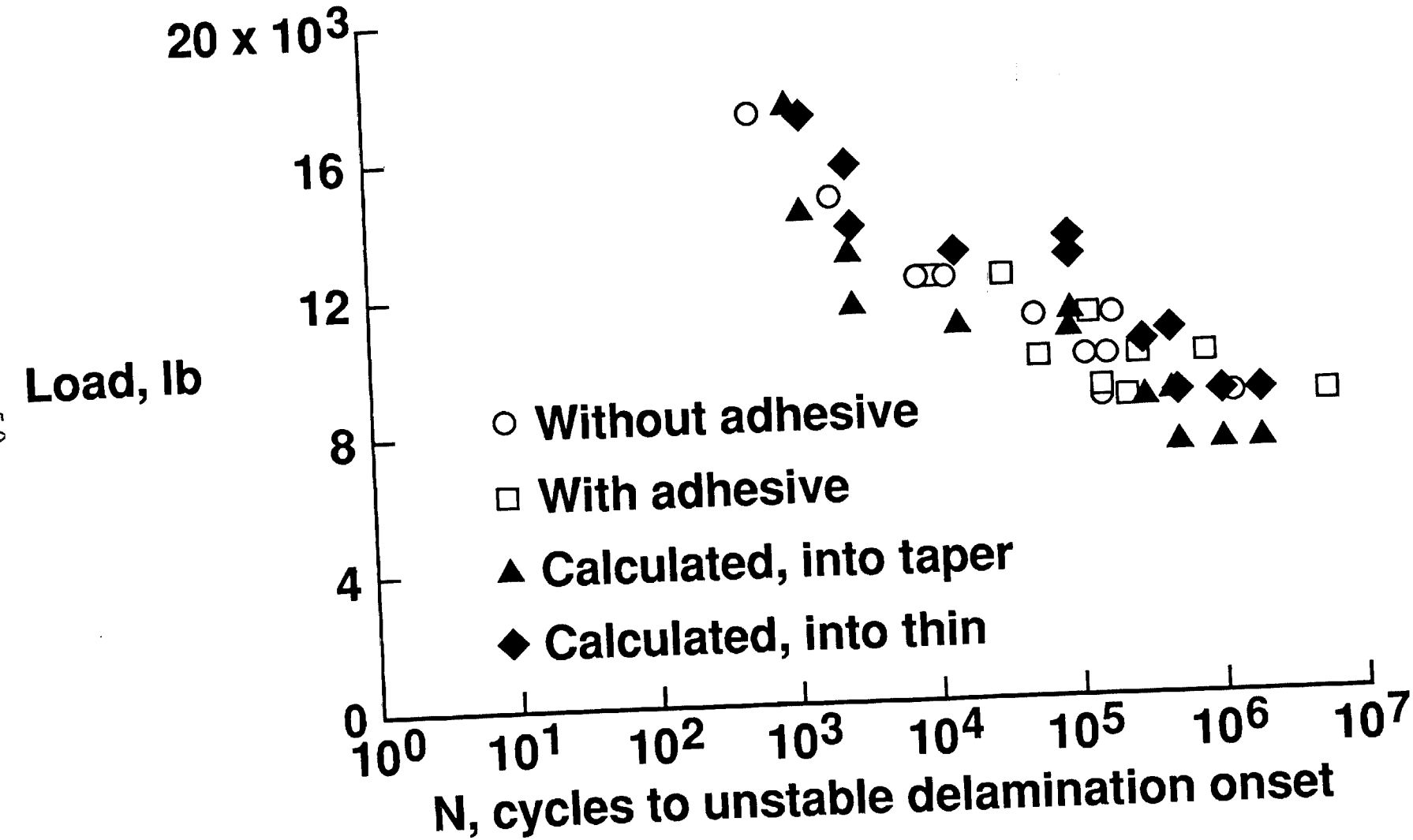

Figure 25. Calculated and measured delamination onset loads for S2/SP250 layup A laminates.

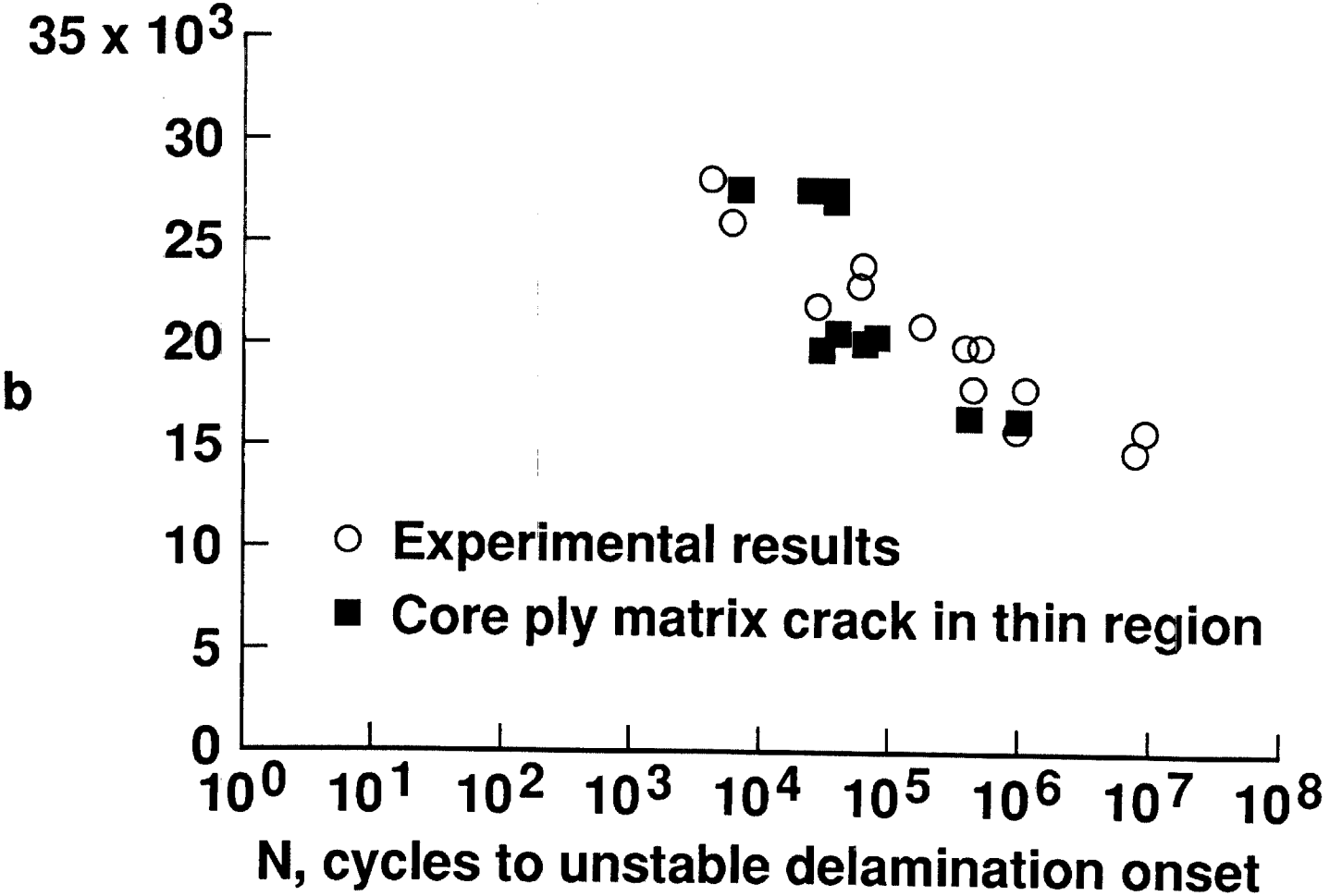

Figure 26. Calculated and measured delamination onset loads for IM6/1827I layup A laminates with ply crack in thin region.

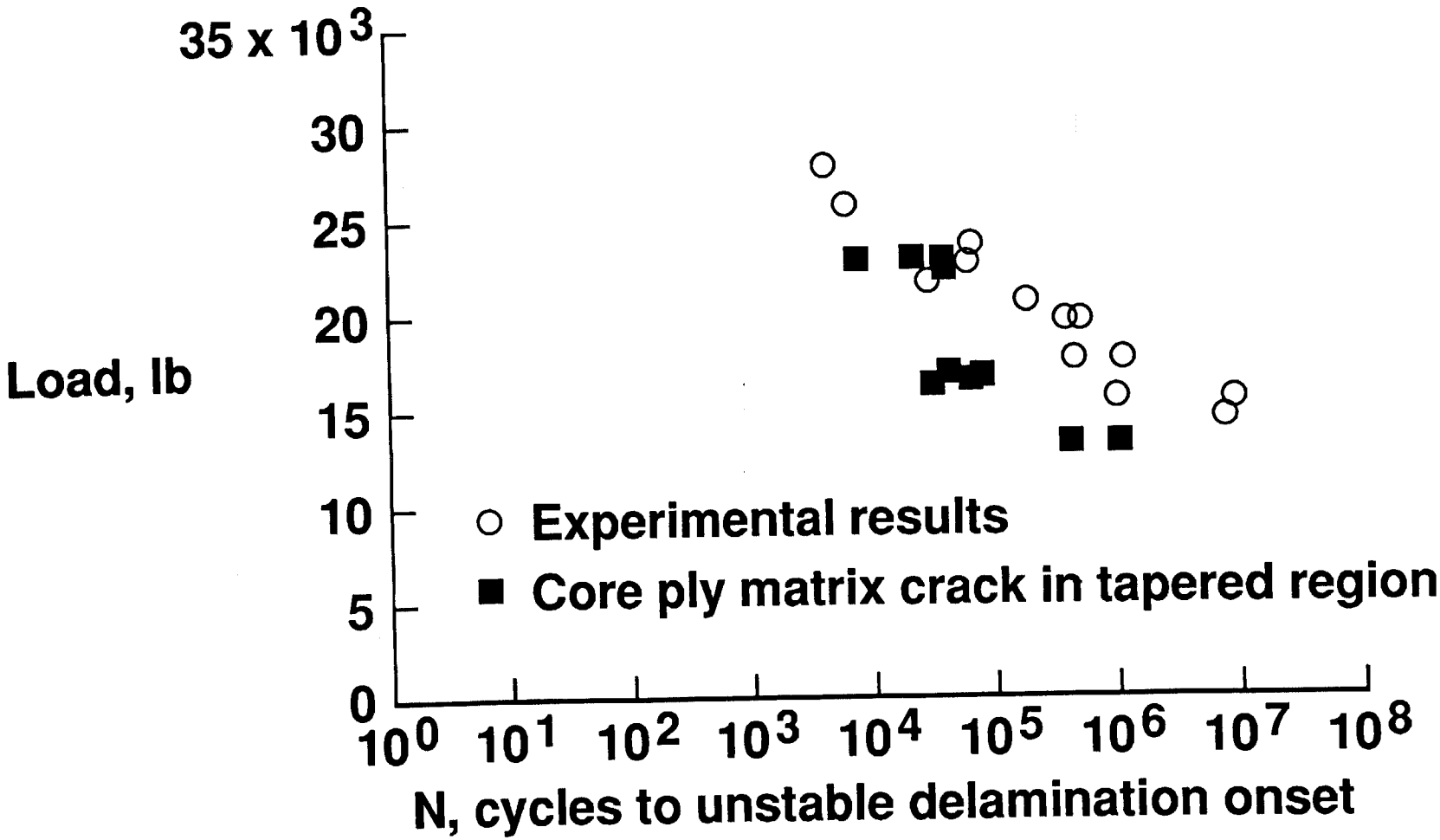

Figure 27. Calculated and measured delamination onset loads for IM6/1827I layup A laminates with ply crack in tapered region.

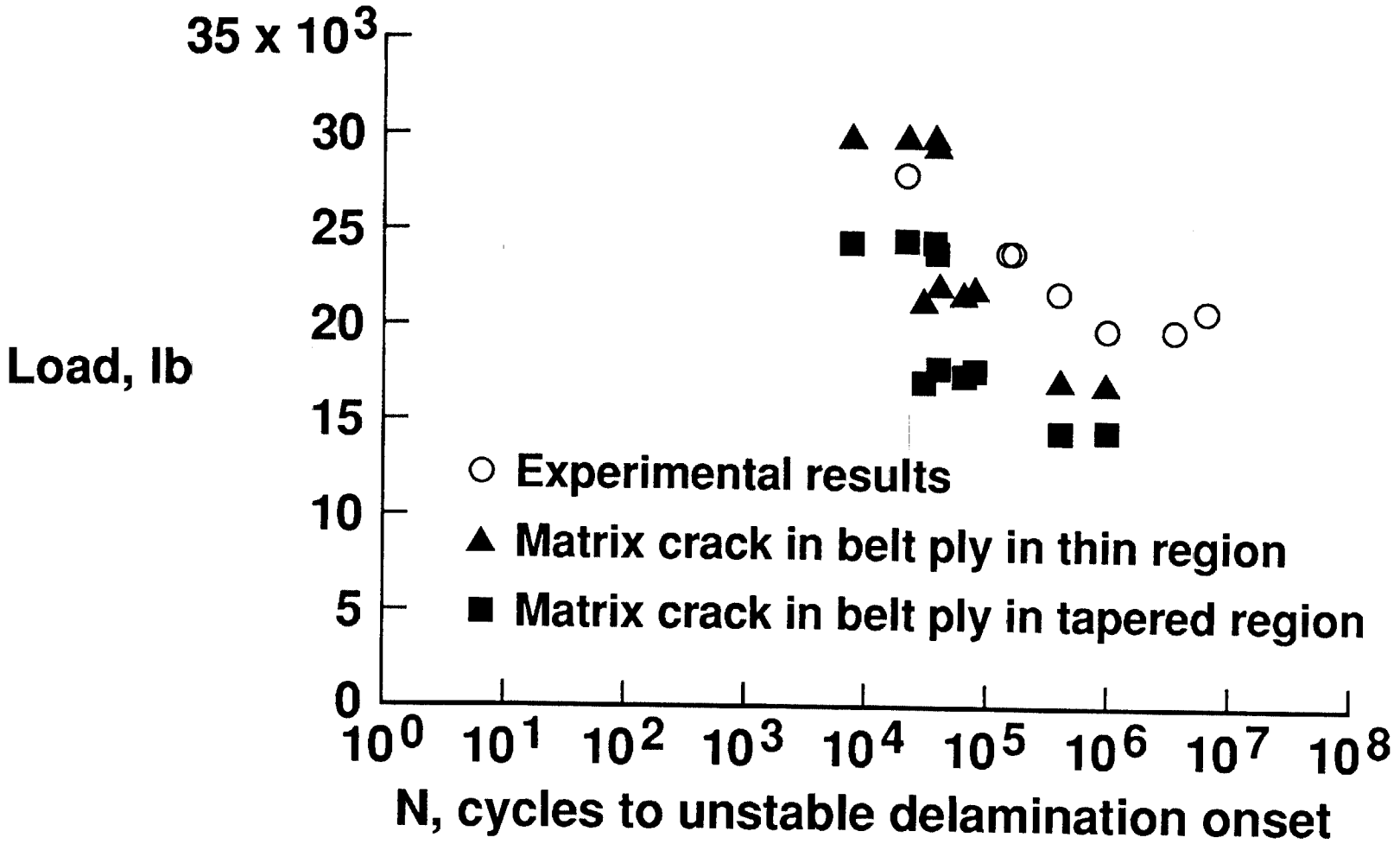

Figure 28. Calculated and measured delamination onset load in IM6/1827I layup B laminates with interleaf at ABCD.

NASA National Aeronautics and Space Administration

Report Documentation Page

1. Report No.	2. Government Accession No.	3. Recipient's Catalog No.
NASA TM-102628 AVSCOM TM-90-B-005		

4. Title and Subtitle

Tension Fatigue of Glass/Epoxy and Graphite/Epoxy Tapered Laminates

5. Report Date

April 1990

6. Performing Organization Code

7. Author(s)

Gretchen B. Murri*; T. Kevin O'Brien*;
and Satish A. Salpekar**

8. Performing Organization Report No.

10. Work Unit No.

505-63-01-05

9. Performing Organization Name and Address

NASA Langley Research Center, Hampton, VA 23665-5225
U.S. Army Aviation Research and Technology Activity (AVSCOM)
Aerostructures Directorate
Hampton, VA 23665-5225

11. Contract or Grant No.

13. Type of Report and Period Covered

Technical Memorandum

12. Sponsoring Agency Name and Address

National Aeronautics and Space Administration
Washington, DC 20546-0001
U.S. Army Aviation Systems Command
St. Louis, MO 63166

14. Sponsoring Agency Code

15. Supplementary Notes

*U.S. Army Aerostructures Directorate, USAARTA-AVSCOM
**Analytical Services and Materials, Inc., Hampton, VA

16. Abstract

Symmetric tapered laminates with internally dropped plies were tested with two different layups and two materials, S2/SP250 glass/epoxy and IM6/1827I graphite/epoxy. Layup A was a $[0_9/(\pm45)_3/(\pm45)_2]_S$ laminate that reduced to a $[0_9/(\pm45)_2]_S$ laminate by dropping the $(\pm45)_3$ plies. Layup B was a $[0_7/\pm45/(\pm45)_3/0/\pm45/0]_S$ laminate that reduced to a $[0_7/\pm45/0/\pm45/0]_S$ laminate in the same manner as layup A. The specimens were loaded in cyclic tension until they delaminated unstably. Each combination of material and layup had a unique failure mode. Calculated values of strain energy release rate, G, from a finite-element analysis model of delamination along the taper, and for delamination from a matrix ply crack, were used with mode I fatigue characterization data from DCB tests of the tested materials to calculate expected delamination onset loads. Calculated values were compared to the experimental results. The comparison showed that when the calculated G was chosen according to the observed delamination failures, the agreement between the calculated and measured delamination onset loads was reasonable for each combination of layup and material.

17. Key Words (Suggested by Author(s))	18. Distribution Statement
dropped plies finite element strain energy release rate Matrix ply crack Delamination	Unclassified - Unlimited Subject Category - 24

19. Security Classif. (of this report)	20. Security Classif. (of this page)	21. No. of pages	22. Price
Unclassified	Unclassified	64	A04

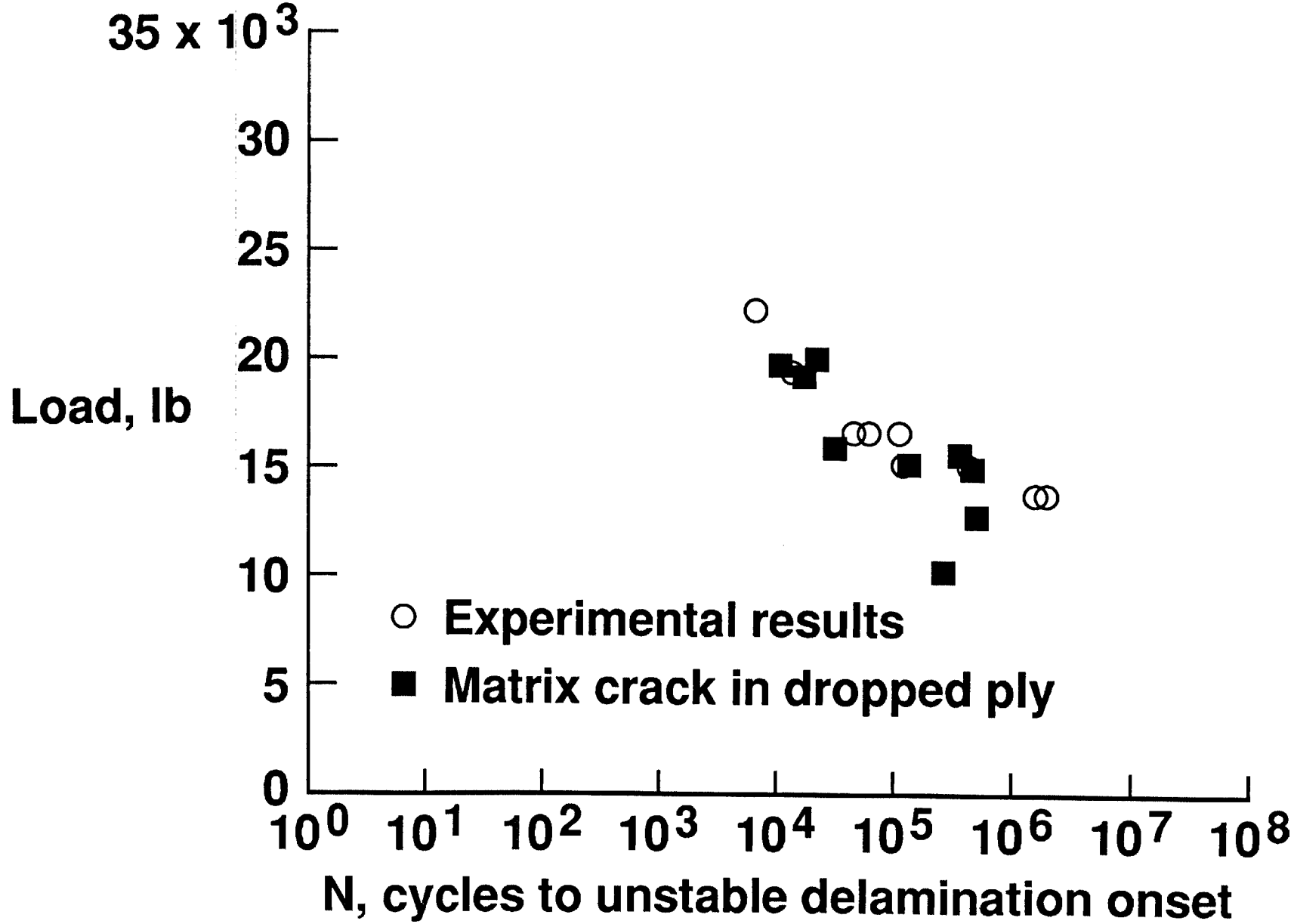

Figure 29. Calculated and measured delamination onset for IM6/1827I layup B laminates without interleaf at ABCD.